공학박사 학위논문

Robust molecular-sieving graphitic membranes for gas and liquid separation

가스 및 용매 분리를 위한 그래핀 멤브레인

2017년 8월

서울대학교 대학원

기계항공공학부

서 동 균

Abstract

Robust molecular-sieving graphitic membranes for gas and liquid separation

Dong Kyun Seo

School of Mechanical and Aerospace Engineering

Seoul National University

Membrane is the most representative technology to solve the environmental crisis facing the world such as global warming, air pollution, depletion of drinking water source by water pollution.

Membrane technology means selectively separating only the desired substances from a mixed gas or solution. The principle of separation uses various principles such as physical, chemical, and mechanical. Primarily, selective separation techniques using size differences of mixed materials are used.

For the recovery of wastewater produced in numerous factories or the recovery of oil spilled into the sea due to accidents, it is necessary to develop a membrane capable of selectively permeating water and oil. The situation in which water and oil are separated from each other frequently occurs and it is a necessary skill to maintain a clean environment.

As the environmental pollution becomes serious, the amount of drinking water that people can drink is decreasing, and the development of new drinking water production technology is imminent due to environmental disasters such as global warming. The technology of converting seawater into freshwater, which accounts for 97% of the Earth, is an essential technology not only for the present but also for the future. Therefore, it is imperative to develop a high-performance membrane that can remove salts.

In addition, the harmful gas generated from the power plant is mostly composed of CO_2, and CO_2 must be separated and collected in the atmosphere as a main cause of global warming. Therefore, it is urgent to develop a membrane fabrication technology capable of separating only desired gases such as CO_2 from various gas molecules.

It is necessary to develop high performance membrane technology with various applications. I have developed the CVHT process to improve the membrane performance. Using this process, a film can be produced due to the chemical bonding of graphene with excellent alignment. In this way, a high-performance membrane was prepared by separating the gas and the solution using a graphitic film having a very good structure.

Keywords: graphene, graphene oxide, hydrothermal, confined 'vapor-phase' hydrothermal, gas separation, liquid separation

Student Number: 2010-30965

Contents

List of Tables

List of Figures

Figure 5-9. (a) Water content of electrolyte after cycling filtration. (b) Water content of electrolyte about acidity test.

Chapter 1. Introduction

Graphene is a nanomaterial consisting of a single layer of carbon atoms and has electrical, physical, chemical and mechanical properties [1-3]. Research has been conducted on the application of such properties to electrodes of electrochemical cells, materials of electric devices, transparent electrodes, adsorbents and membranes [4-7].

It has a two-dimensional shape and it is possible to manufacture various structures. We are studying the applicability of nano wire or high performance electrode or heat emission material by fabricating it as one dimensional wire shape. In addition, studies have been made to fabricate a three-dimensional structure and achieve a porous shape and use it as an electrode of an adsorbent or a supercapacitor [8, 9]. This is a structure made of nanoparticles of graphene, which has a large specific surface area, so it can have a higher charge and discharge capacity than other materials.

In order to fabricate a two-dimensional structure, a large number of mechanical and physical methods are being studied in the laboratory to

improve the performance of the membrane by uniformly laminating the graphene in the plane direction. In order to improve the performance of the membrane, it is important to complicate the movement path of the substance to be separated or to manufacture a passage of a uniform size [10-13]. It may also take advantage of chemical bonding or solubility differences with the separation material. There is a growing interest in graphene as a material for the membrane to increase the separation. Growth of graphene is disadvantageous because it is difficult to fabricate large area and it is difficult to stack multiple layers of graphene. On the other hand, graphene oxide (GO) produced from graphite through oxidation process can be mass-produced, and it is possible to produce uniform size GO by controlling process variables.

Techniques for fabricating membranes using GOs with these advantages are under development, which typically utilize mechanical lamination processes. GO alone and it is not possible to achieve uniform lamination. However, the development of a technology capable of ideally uniform lamination has not yet been developed. Research is underway to apply this technique to the

separation of gases or solutions using GO-based membranes with these limitations. The lack of superior performance compared to membranes using conventional polymers is due to the structural limitations of GO-based membranes [14-16].

In order to solve this problem, I developed a new technology to fabricate a high performance GO membrane. We have developed a confined 'vapor-phase' hydrothermal (CVHT) process by improving the existing hydrothermal process. If the existing hydrothermal process was a technique for fabricating a porous graphene structure, the new CVHT process is a technique for fabricating a structure in which graphene is evenly stacked on the entire surface.

Using the CVHT process, a graphene film with uniform lamination as well as physical bonding as well as physical bonding was fabricated. Using this, a membrane was prepared to separate carbon dioxide, nitrogen, carbon dioxide and methane. Membranes were fabricated to remove water impurity from the electrolyte, which hinders cell performance in lithium ion batteries.

Chapter 2. Graphene oxide synthesis

In this chapter, we will refer to the technology of making graphene oxide (GO) as a material for the membrane. The oxidation process and the properties of the prepared GO are verified by various analytical methods. In addition, we will confirm the physical properties of GO prepared by our laboratory compared with the existing GO production process.

2.1. Properties of graphene oxide

2.1.1. Graphene oxide

Graphene oxide is a typical graphene production method because it can be mass-produced in the graphene production method and it is easy to produce graphene of uniform quality [17-20]. Through the oxidation process, the gap between pure grains inside graphite is widened. After this, a single piece of graphene can be obtained using a mechanical stripping method. Due to the oxidation process, various oxygen-related functional groups are formed on the surface and edge of graphene. The types and patterns of functional groups attached to the GO are shown in Figure 2-1 [21]. Through various modeling, the shape of the GO after the oxidation process was investigated and reported by many research teams.

Pure graphene has a thickness of 0.4 nm. This is the thickness of a sheet of graphene composed of carbon hexagonal structure, which is reported by many research teams. However, when the oxidation process is performed to fabricate the GO, atomic force microscopy (AFM) confirms that the actual

thickness increases with the attachment of functional groups on both sides of the graphene (Fig. 2-2 (a)). It can be seen from the graph that the thickness of GO is increased to the level of 0.8 ~ 1 nm. In addition, tunneling electron microscopy (TEM) shows that many defects such as pores are formed on the graphene surface through the oxidation process (Fig. 2-2 (b, c)). It can be seen from the image that voids are formed due to the deviation of the carbon atoms from the carbon hexagonal structure, which is a disadvantage of the GO generation process [22-25].

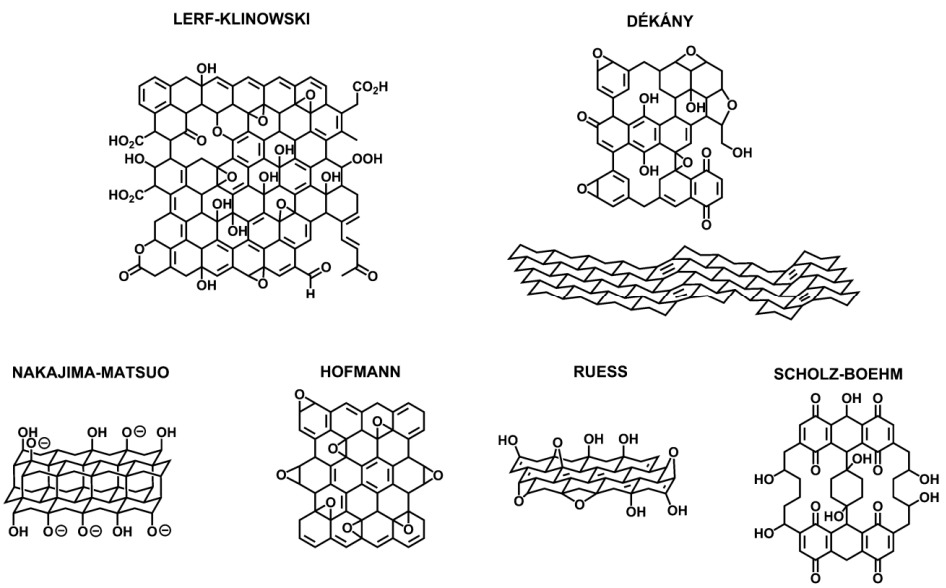

Figure 2-1. Structural models of GO that have been proposed.

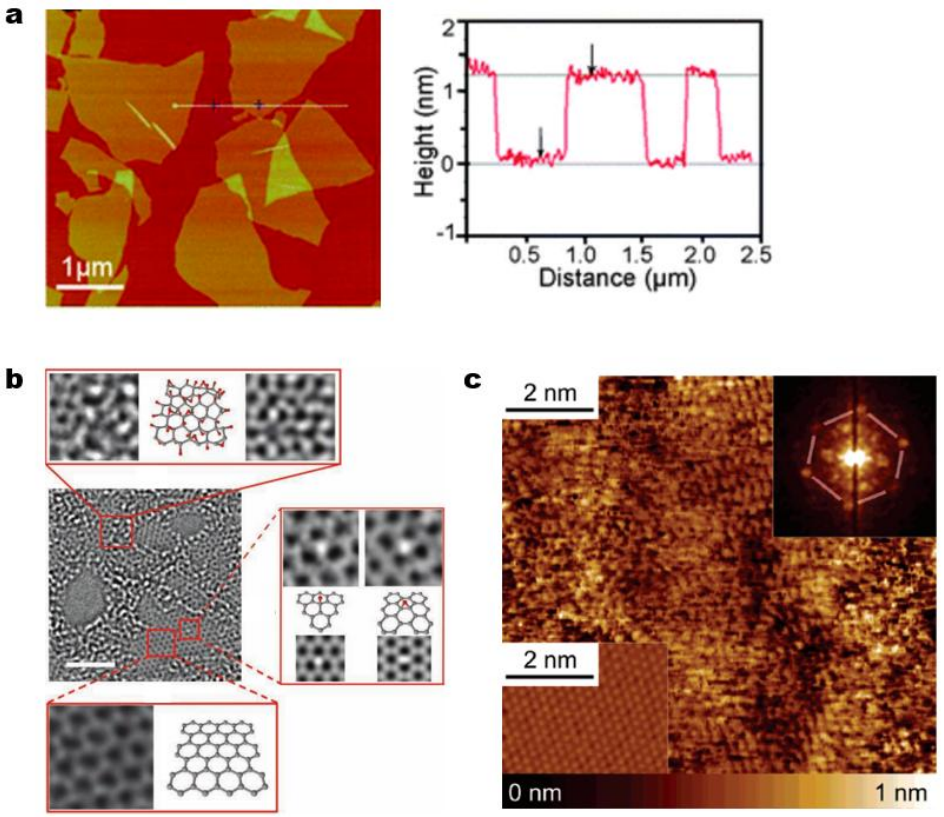

Figure 2-2. (a) AFM image of GO. (b) Aberration-corrected TEM image of GO. The scale bar is 2 nm. (c) STM image of GO. Inset on the right top is the Fourier transform of the image. Inset on the left bottom is the image of highly oriented pyrolytic graphite.

The chemical composition of GO has been investigated using a variety of spectroscopies including solid-state nuclear magnetic resonance spectroscopy (SSNMR), X-ray photoelectron spectroscopy (XPS), Raman spectroscopy, and Fourier transform infrared spectroscopy (FT-IR) as shown in Figure 2-3. Predominant chemical bonds in GO are identified to be C=C (sp^2 carbon), C-OH (hydroxyl group), C-O-C (epoxy group), C=O (carbonyl group), and COOH (carboxyl group). The degree of oxidation is dependent on synthesis methods of GO (oxidant agents, oxidation time, and temperature) [26-28]. The oxygen content of GO typically ranges from 20 to 40 at%. Abundant oxygen functional groups provide chemically reactive sites for functionalization and make aqueous GO colloidal solution stable.

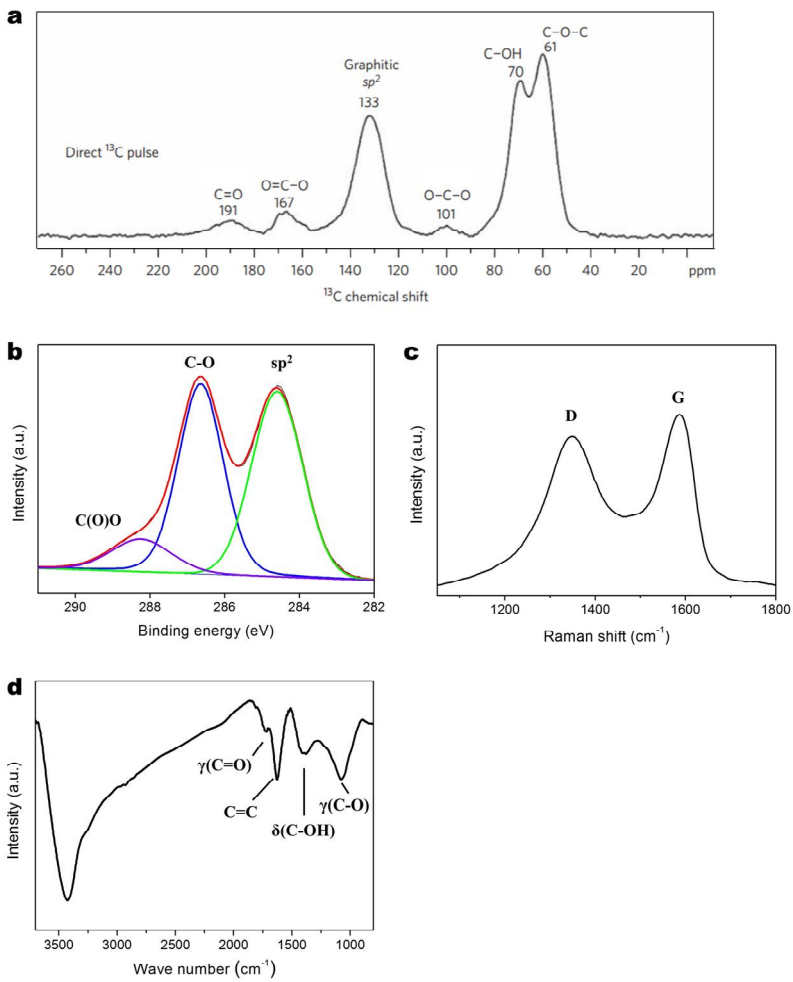

Figure 2-3. (a) SSNMR spectrum of GO. (b) XPS spectrum of GO. (c) Raman spectrum of GO. (d) FT-IR spectrum of GO.

2.1.2. Mechanical property of graphene oxide

The mechanical strength of the GO is measured using a 2-dimensional or 3-dimensional structure. Vacuum filtration is mainly used for fabrication of two-dimensional structures. A GO paper is prepared by depositing GO, which is dispersed in water or organic solvent, on the filter. As can be seen in figure 2-4 (a), the prepared GO paper has uniform thickness and roughness. Also, the paper size can be adjusted by the size of the filter. The thickness of the paper can be controlled by the amount of GO to be filtrated (Figure 2-4 (b)). As can be seen from figure 2-4 (b), we can confirm the lamination behavior of GO on the cross section of the paper. It can be seen that the GO is stacked evenly in the thickness direction according to the filtration direction [29-33].

When the filtration is used, the mechanical strength of the GO paper is weak because the adjacent GO bonds with only van der waal's force. Also, even if the film produced by filtration is dried, water molecules trapped in the GO are not easily separated from the GO due to the hydrophilic nature of the GO. This can be confirmed by changing the d-spacing of GO paper through

heat treatment (Figure 2-4 (c)). Through the X-ray diffraction (XRD), the gap between the GOs in the GO paper can be known. It can be seen that the d-spacing decreases with the heat treatment. It can be seen that the gap is reduced by the dehydration reaction in GO paper and actually affects the mechanical strength of the paper. The mechanical strength of the paper produced by vacuum filtration can be seen in figure 2-4 (d). As described above, it can be confirmed that the strength of the paper is changed by the heat treatment. As the heat treatment temperature rises, the number of water molecules desorbed increases, which leads to the effect of increasing the bond strength of the paper. This shows that young's modulus and tensile strength are increased.

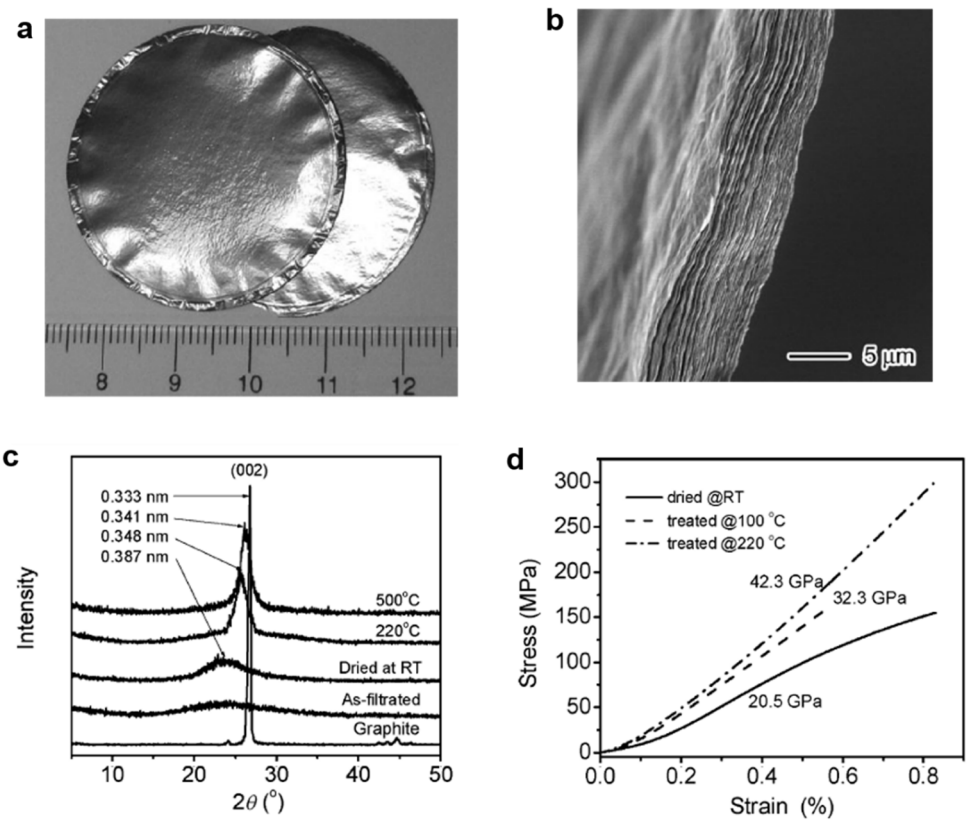

Figure 2-4. (a) GO paper using vacuum filtration. (b) SEM image of GO paper side. (c) XRD data of GO papers by heat treatment. (d) Mechanical strength of GO papers.

One of the ways to measure the mechanical strength of a GO is to fabricate the structure and measure its strength. In order to measure the tensile strength, there is a method of measuring the strength of a film by making a two-dimensional film and applying tension to both sides. On the other hand, when a three-dimensional structure is manufactured, not only tensile but also compressive strength can be measured. Since mechanical properties measured when compressing the structure are related to recovery, it can be an important criterion when evaluating the properties of GO [34-37].

As can be seen in figure 2-5 (a), a graphene-based three-dimensional structure can be fabricated using a hydrothermal process. It is made by chemical bonding between graphenes in water and is a combination of graphenes dispersed in water. In addition, since the structure is made in water, it is made in a hydrogel state, and a structure in which water occupies more than 95% of the volume of the structure is produced [38-39].

As can be seen in figure 2-5 (b), it can be seen that the shape of the fabricated structure is retained even in the state of aerogels in which water is

removed through freeze-drying. It can be seen that the bonding force of the graphene constituting the structure is very good. In addition, it can withstand loads of more than 100 times its mass (Figure 2-5 (b)).

In figure 2-5 (c), the viscosity of the structure was measured by compression test. In order to confirm the bonding force and the bonding structure due to the bonding between the graphene of the structure, the viscosity of the structure was measured. As can be seen from the graph in figure 2-5 (c), the shear force applied to the hydrogel structure and the shear rate increase indicate that the measured results are similar to those of polymer hydrogel. As the shear rate increases, the graphene bonding force weakens and the graphene bonding acts to lower the viscosity of the structure while sliding (Figure 2-5 (d)). The elastic modulus (G') and the viscous modulus (G") were measured using small-deformation oscillatory measurements, and the value of G' was measured 10 times higher than that of G" (Figure 2-5 (d)). A certain aspect of the angular frequencies was measured and this shows that the hydrogel has a regular and constant structure. In addition, this means

that the graphene is bound by a strong bonding force, and a value of 470 kPa is measured at 10 rad / s G" value [40-45].

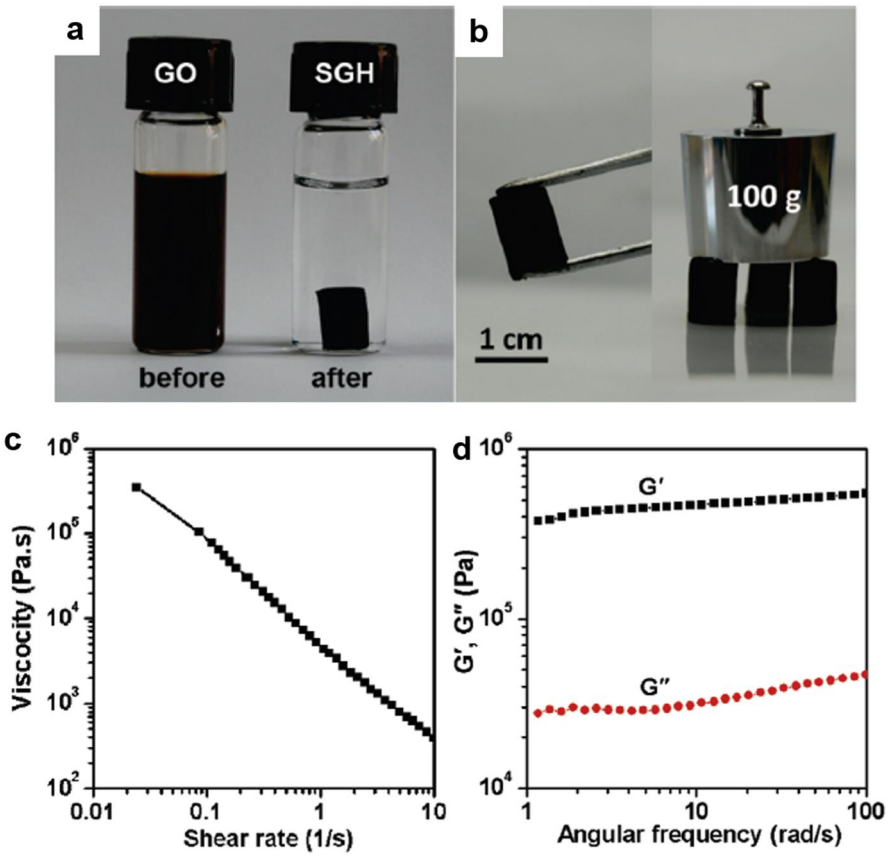

Figure 2-5. (a) Photographs of a homogeneous GO aqueous dispersion before and after hydrothermal reduction. (b) Photographs of a graphene hydrogel allowing easy handling and supporting weight. Steady (c) and dynamic (d) rheological behaviors of the graphene hydrogel.

2.2. Hummers method

2.2.1. Conventional Hummers method

There are three representative methods of making graphene. The first is how to peel off graphene from graphite. It is possible to fabricate pure graphene by removing a single graphene from the adhesive side of the tape when the graphite is contacted with and detached from the adhesive material such as tape. However, such a method has a disadvantage that it is difficult to repeat, is not suitable for mass production, and is difficult to commercialize. A second way to fabricate graphene is to grow graphene directly (Figure 2-6). Graphene utilizes the solubility characteristics of carbon atoms in copper metal. The principle is to utilize the principle that graphene grows as the carbon atoms dissolved into the copper precipitate on the metal surface. With this method, pure graphene can be fabricated and a large-area graphene can be produced by a roll-to-roll process as shown in Figure 2-6(a). By controlling fabrication process parameters, it is possible to fabricate multiple graphenes in a single graphene. On the other hand, as shown in

figure 2-6 (b), there is a disadvantage that complicated equipment is required. In addition, it has a disadvantage that a high temperature condition of 1000℃ or more is required. A CVD apparatus equipped with a chamber capable of maintaining a temperature of 1000℃ and a vacuum state is required. In addition, since graphene must be grown on a metal substrate, another process is required for transferring the graphene to another substrate. And the graphene defects due to the boundary of the substrate must be generated. Due to these disadvantages, the applicability of graphene grown in CVD is limited. Since it can be applied to a transparent electrode, it has an advantage that it can be applied to various displays. However, it has a disadvantage that it is difficult to find applications other than display [46-50].

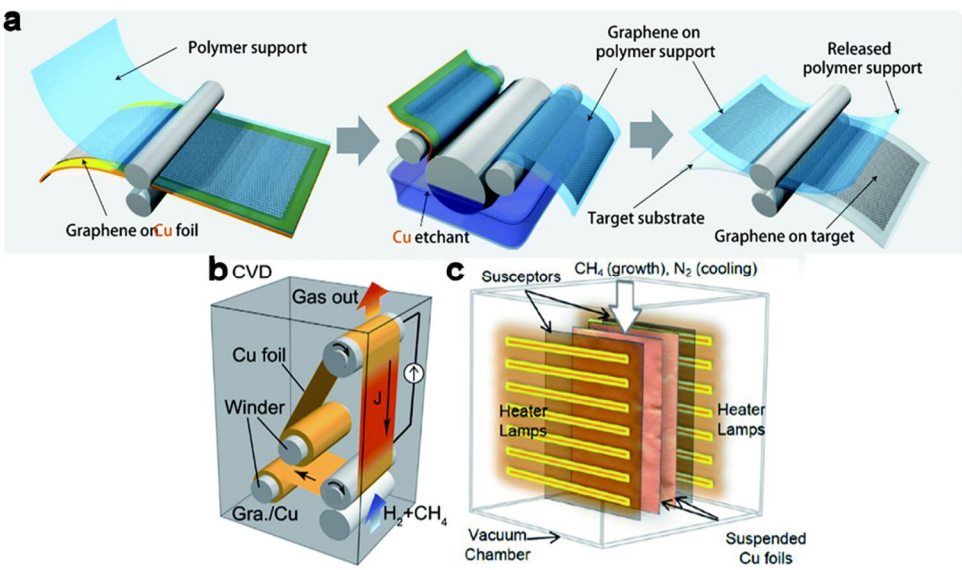

Figure 2-6 (a) Schematic diagram of the roll-to-roll production of graphene film. (b) Schematic diagram of R2R CVD system using selective joule heating. (c) Schematic illustration of RT-CVD synthesis setup.

2.2.2. Modified Hummers method

To overcome the disadvantages of this graphene fabrication process, a technique has been developed for collecting graphene directly from graphite. The graphite is oxidized by Hummers method to make graphene (Figure 2-7 (a)). The basic method of the Hummers method is to oxidize the graphene graphene layer to widen the gap between graphenes. Among the methods of widening the gap between graphenes, there is a method of sandwiching metal ions between graphenes, but this method has a disadvantage of removing metal particles attached to graphene surface after graphening. Therefore, it is the method that most research team is carrying out the technique of collecting graphene through simple oxidation process [51-53].

Use potassium permanganate ($KMNO_4$) to accelerate the oxidation process (Figure 2-7 (a)). When this method is used, the acidity of the acid used for the oxidation is increased and the oxidation of the graphite is promoted. Many researchers have used a variety of catalysts to increase the oxidation level, but in general Hummers methods use $KMNO_4$.

Although the graphene produced by such an oxidation process falls into a single graphene, it is formed on the surface of the graphene by the oxidation of functional groups. Since the carboxyl, epoxy and carbonyl groups are attached to the surface of graphene, the graphene produced is called graphene oxide. In addition, the thickness of GO is thicker than that of general graphene, and it has a thickness of 0.7 ~ 1 nm (Figure 2-7(b)).

In addition, although the gap between graphite is increased through oxidation, a sonication process must be performed to obtain a single graphene. Through this process, graphene is separated and torn. The GO has a lateral size of 1 ~ 10 μm [54].

Graphene oxide, which has a shape with an aspect ratio of about 1000, has a variety of applications. As well as. The hummers method has the advantage of mass production of GO and low unit price.

On the other hand, since the GO is produced by using the oxidation process, the GO has a disadvantage of not having the electric conductivity. To solve this problem, various studies have been conducted to reduce GO. A

reduction method using heat treatment as well as a chemical reduction method using hydrazine has been studied [55-59].

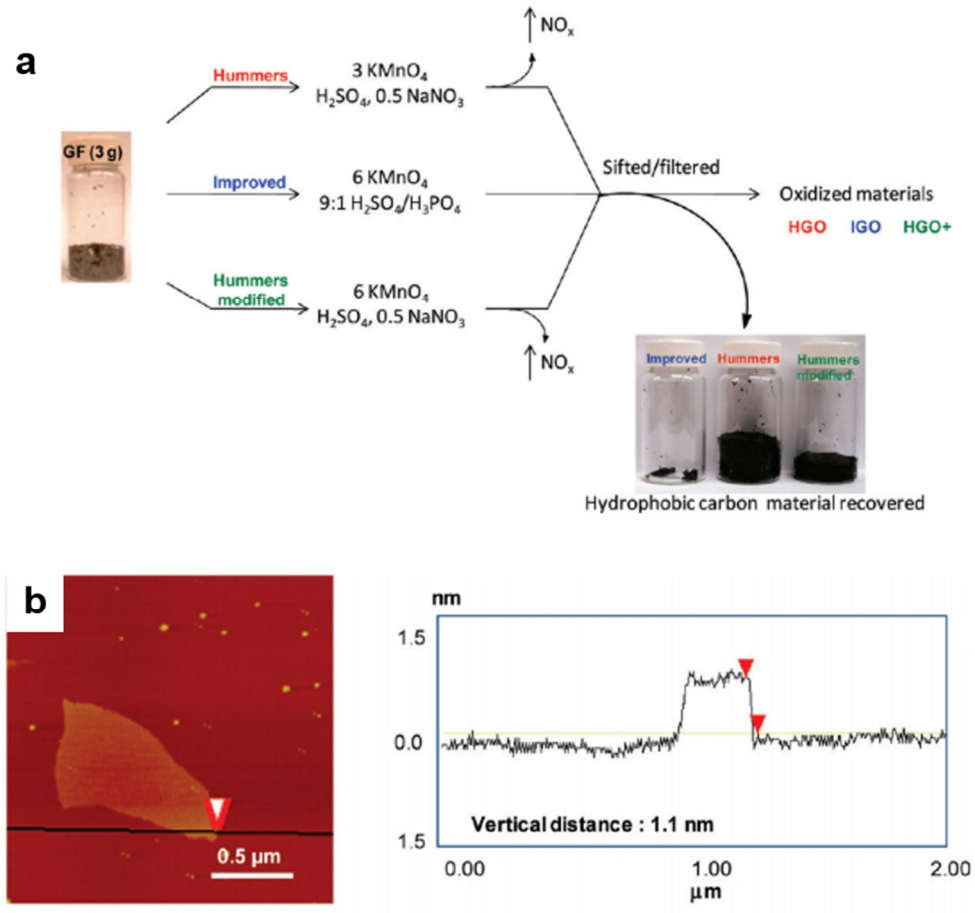

Figure 2-7. (a) Representation of the procedures followed starting with graphite flakes. Under-oxidized hydrophobic carbon material recovered during the purification. (b) Tapping mode AFM topographic images and height profiles of a single layer.

Using graphite purchased from bay carbon, 0.3 g of graphite add 1.8 g of $KMNO_4$ and add 40 ml of sulfuric acid. The solution is heated to 40-60℃ in a water bath and stirred for 6 hours. In this process, the graphite is oxidized and the gap between the graphenes is widened. Due to the high reactivity of $KMNO_4$, which acts as a catalyst for oxidation, it should not be heated above 60℃.

Water is added to neutralize the solution with high acidity. When a large amount of water is added at a time, a small amount of water is added dropwise, since the oxidized graphene may be reduced by heating at a high temperature. The temperature of the solution should be kept below 10℃.

Add 30 ml of hydrogen peroxide to remove remaining $KMNO_4$ in the solution. H2O2 reacts with $KMNO_4$ and dissolves in water in water or evaporates into gas [60-62].

In addition, the acidity of the solution can be lowered by passing the neutralization process several times, and the prepared GO can be dispersed in water.

Finally, GO paper is prepared by using vacuum filtration process. The paper

is dried in a vacuum chamber heated at 70℃ for 24 hours. Once this process is completed, a fully dried GO paper can be produced.

In order to disperse the prepared GO paper in water at a certain concentration, the precise mass is measured, and the resultant is added to water and then the sonication process is carried out. At this time, the oxidized graphene is completely separated into one sheet. Since the graphene is mechanically removed, the graphene is torn. The lateral size of torn graphene is about 1 μm. The sonication process can be performed for 1 to 3 hours to produce uniform size GO [63-67].

In this way, homogeneous GO can be fabricated by using optimized modified Hummers method (Figure 2-8).

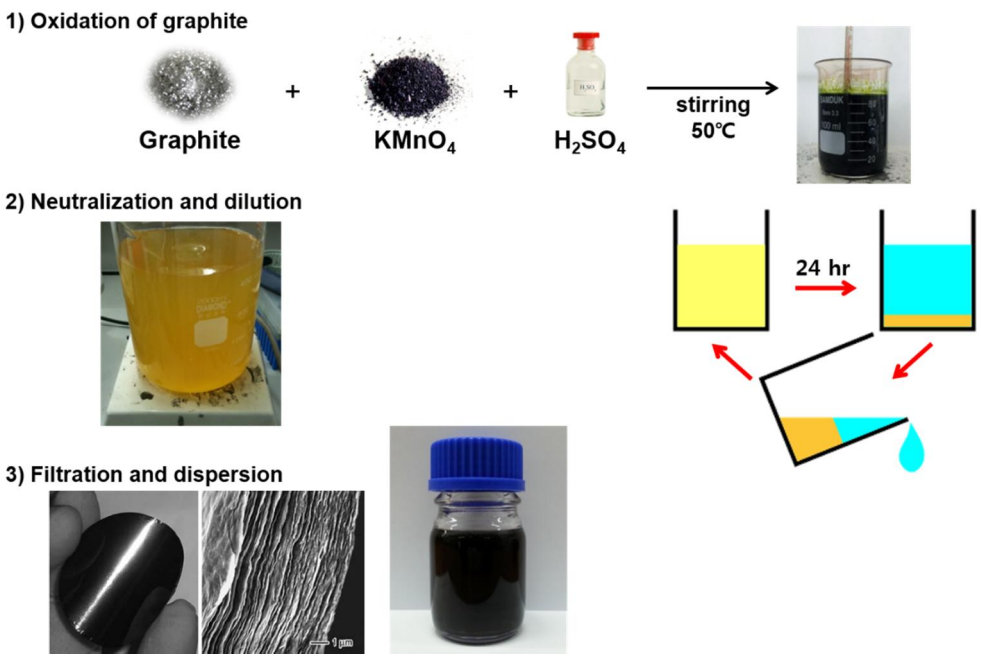

Figure 2-8. Schematic of modified Hummers method.

2.3. Basic properties of GO

2.3.1. Morphology

The shape of the GO can be seen in figure 2-9. It can be seen that the size of the GO is made to 1 μm level through the sonication process. It can be seen that the lateral size of the prepared GO is variously distributed from several hundred nm to 1 μm [68-70].

Mica was used to measure the exact size of the GO. Mica has a structure similar to graphite. One layer of mica with layered structure has a uniform roughness of 1 Å level. Therefore, accurate thickness of GO can be measured by using mica as a substrate [71-73]. In addition, the GO dispersed in water was dropped on the mica substrate to prepare specimens. Using this process, it is easy to measure the GO thickness because the GO is uniformly distributed on the mica and coated on the mica substrate without leaving.

The size of a typical graphene is known to be 0.3 nm. The graphite graphene also has the same thickness as the graphene grown by CVD. However, it can be seen that the GO made by the modified Hummers method has a thicker thickness of 1 nm.

This is because various functional groups attach to both sides of the graphene through the oxidation process. Oxygen - related functional groups such as carboxyl, epoxy and carbonyl groups were attached to increase the thickness of graphene. The increased thickness of grapehen has a thickness of about 1 nm, which is equivalent to the thickness of GO reported by many researchers. This means that the modified Hummers method can produce homogeneous GO.

On the other hand, reduced graphene oxide (rGO) can be produced by reducing GO using hydrazine. GO does not have electrical conductivity because surface and edge are oxidized and functional groups are attached. This is not suitable for use in a variety of applications, so it is necessary to restore electrical conductivity using a reduction process. For this, when

hydrazine is added to GO solution and heat treatment is performed, the functional group of GO is desorbed and reduced, and the thickness becomes thinner. This can be seen in figure 2-10.

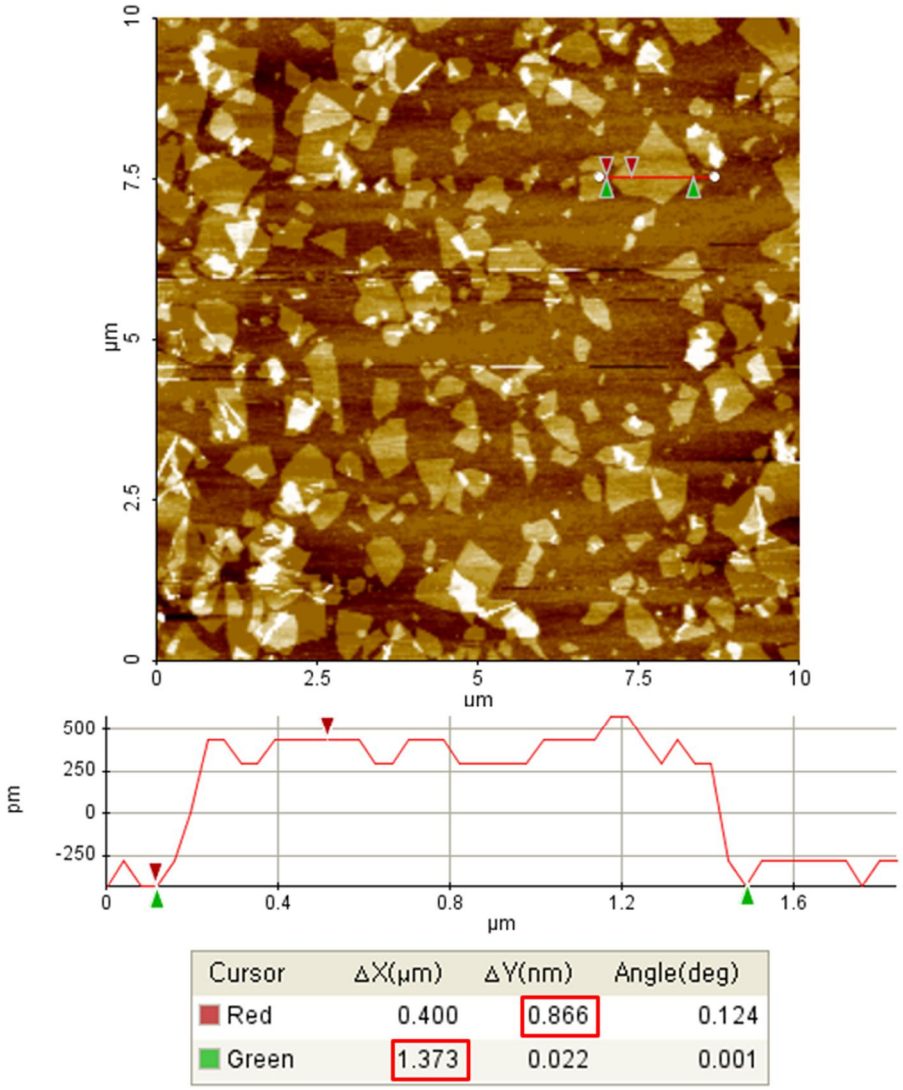

Figure 2-9. AFM image of GO.

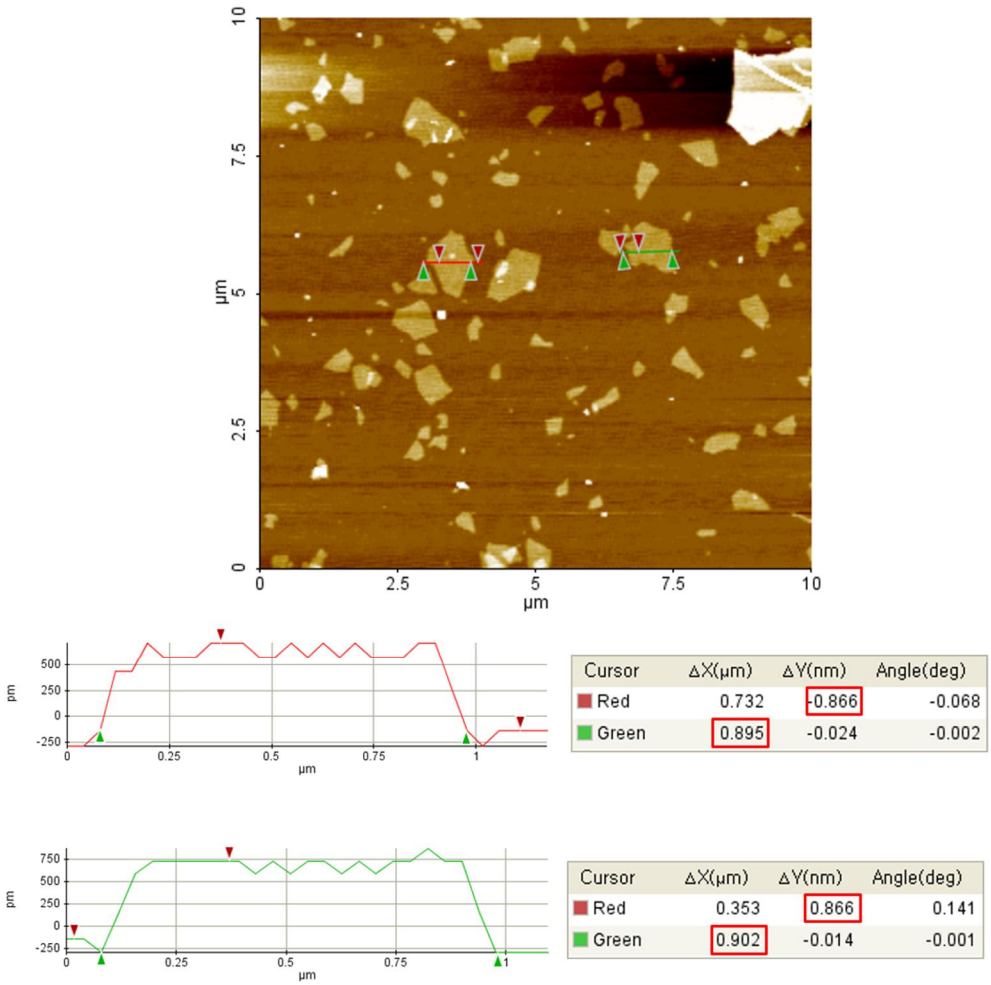

Cursor	ΔX(μm)	ΔY(nm)	Angle(deg)
Red	0.732	-0.866	-0.068
Green	0.895	-0.024	-0.002

Cursor	ΔX(μm)	ΔY(nm)	Angle(deg)
Red	0.353	0.866	0.141
Green	0.902	-0.014	-0.001

Figure 2-10. AFM image of rGO.

2.3.2. Chemical structure

The assignment of peaks in the O1s spectra is of interest, as there are some conflicting assignments of the "carbon–oxygen" functional groups in the literature. Information provided by analysis of the O1s spectra can complement the information provided by analysis of C1s spectra. Because the O1s photoelectron kinetic energies are lower than those of the C1s, the O1s sampling depth is smaller, and therefore the O1s spectra are slightly more surface specific. By reference to the C1s peak changes, we have assigned the O1s peak at 530.6 eV to contributions from C=O and O=C–OH groups and that at 533 eV to C–OH groups [74-78]. After annealing, the peak at 530.6 eV shifts to lower binding energy (ranging from 529.6 to 529 eV, depending on the thermal treatment), which indicates a conversion of the C=O and O=C–OH groups to a new chemical species. Whereas, the peak at 533 eV does not appear to shift appreciably at these anneal temperatures. The complete disappearance of all peaks other than the 533 eV peak after the 1000℃ treatment indicates loss of oxygen (and possibly carbon) during the high temperature treatments. The remaining peak at 533 eV indicates

that C–OH groups are still present. It is perhaps of interest that the authors of theoretical calculations reach the conclusion that the reduction of remaining C–OH groups in a reduced graphene oxide is very difficult, although reduction of some initial fraction of the C–OH groups in the as-prepared graphene oxide is more facile. It is noted that a slight shift of 0.25 eV to lower binding energy is observed for the peaks of both the C1s and O1s spectra after the 1000℃ anneal, which indicates that there was some sample charging in the spectra for GO and the lower temperature anneals.

In graphene, the Stokes phonon energy shift caused by laser excitation creates two main peaks in the Raman spectrum: G (1580 cm^{-1}), a primary in-plane vibrational mode, and 2D (2690 cm^{-1}), a second-order overtone of a different inplane vibration, D (1350 cm^{-1}) (Figure 2-12). D and 2D peak positions are dispersive (dependent on the laser excitation energy). The positions cited are from a 532 nm excitation laser. Because of added forces from the interactions between layers of AB-stacked graphene, as the number of graphene layers increases, the spectrum will change from that of single-layer graphene, namely a splitting of the 2D peak into an increasing number

of modes that can combine to give a wider, shorter, higher frequency peak. The G peak also experiences a smaller red shift from increased number of layers. Thus, for AB-stacked graphene, the number of layers can be derived from the ratio of peak intensities, I2D/IG, as well as the position and shape of these peaks. Rotationally disordered (decoupled) multilayer graphene, however, can still have a single intense 2D peak regardless of thickness, though its position and FWHM can depend on the number of layers [79-83].

Using the ratio of peak intensities ID/IG, one can use Raman spectra to characterize the level of disorder in graphene. As disorder in graphene increases, ID/IG displays 2 different behaviors. There is a regime of "low" defect density where ID/IG will increase as a higher defect density creates more elastic scattering. This occurs up to a regime of "high" defect density, at which point ID/IG will begin to decrease as an increasing defect density results in a more amorphous carbon structure, attenuating all Raman peaks [84-85].

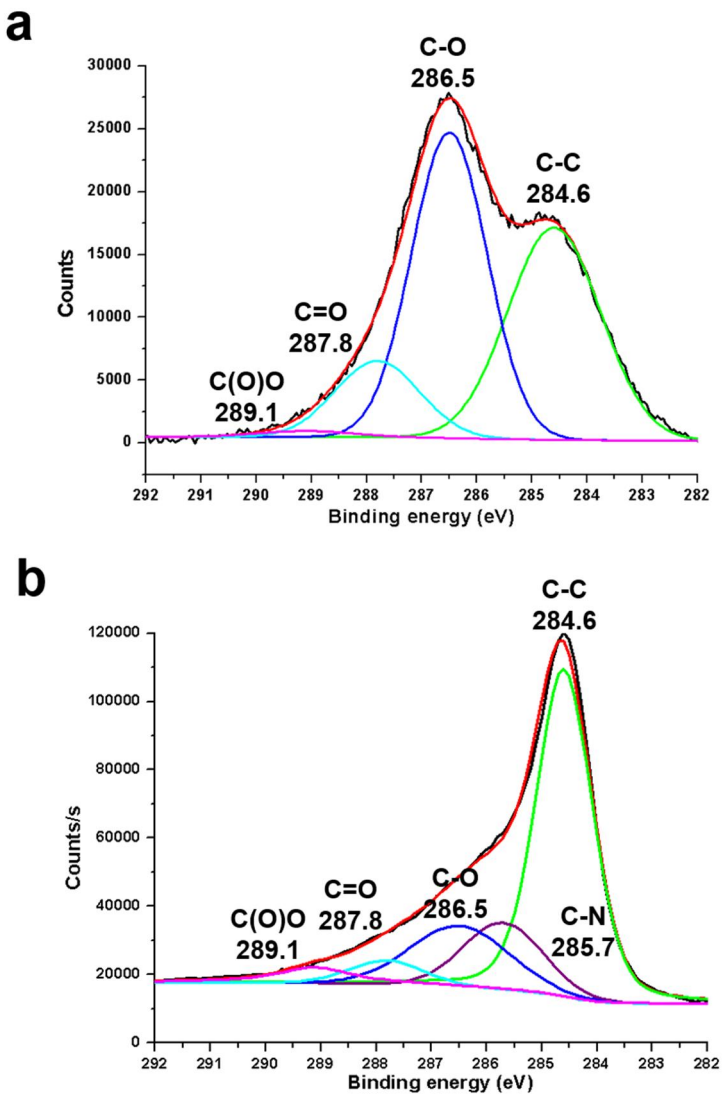

Figure 2-11. XPS analysis of (a) GO. (b) rGO.

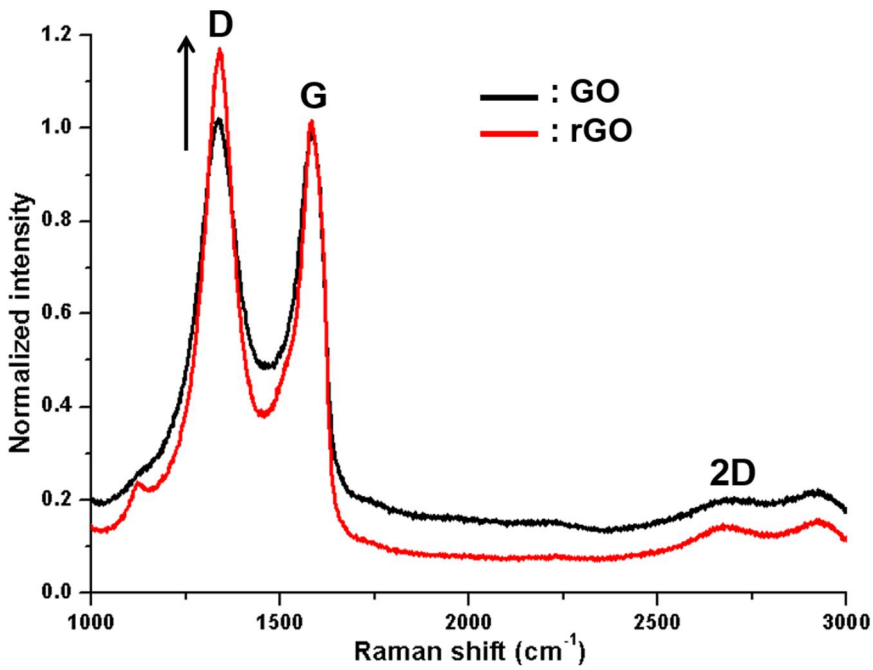

Figure 2-12. Raman analysis of (a) GO. (b) rGO.

Chapter 3. Confined ‘vapor-phase’ hydrothermal process

This chapter introduces new methods that are completely different from the existing hydrothermal processes. If the existing method was to make a porous three-dimensional graphene structure, the method to introduce is to make a graphitic film with high purity alignment. It is a method of producing graphitic film which induces chemical and physical bonding of adjacent graphene and has high mechanical and electrical properties.

3.1. Conventional hydrothermal method

3.1.1. Graphene hydrogel

A typical method for producing graphene-based three-dimensional structures is the hydrothermal method. Graphene-based 3D structures have various applications. Porous structures can be made using graphene with a large specific surface area. The fabricated structure also has a large surface area and can design various sizes of pores using 1 μm graphene. Using these structural advantages, it can be used as electrodes for various batteries and supercapacitors.

In order to utilize this applicability, studies on the fabrication of graphene three-dimensional structures using the hydrothermal method have been carried out predominantly (figure 3-1). As can be seen in the figure, the three-dimensional structure is made in solution, and after the process is completed, it is made in hydrogel form (figure 3-1 (a)). Simply applying a high temperature in a closed container causes the graphene to become

chemically bonded. It is a simple process and has the advantage that it can be used industrially.

Since graphene is dispersed in water, it is anisotropically bonded and graphene bonds to form a structure. This can be confirmed by SEM image (figure 3-1 (a, b)). The graphene combines without directionality and pores are filled with water. If freezing-drying process is used to remove water without deformation of the structure, a three-dimensional structure can be fabricated that is made entirely of graphene.

The structure has excellent mechanical strength (figure 3-1 (b)) because it induces chemical bonding of graphene at the same time as reduction in superheated water. You can build a sturdy structure that can weigh hundreds of times the weight of the structure [86-90].

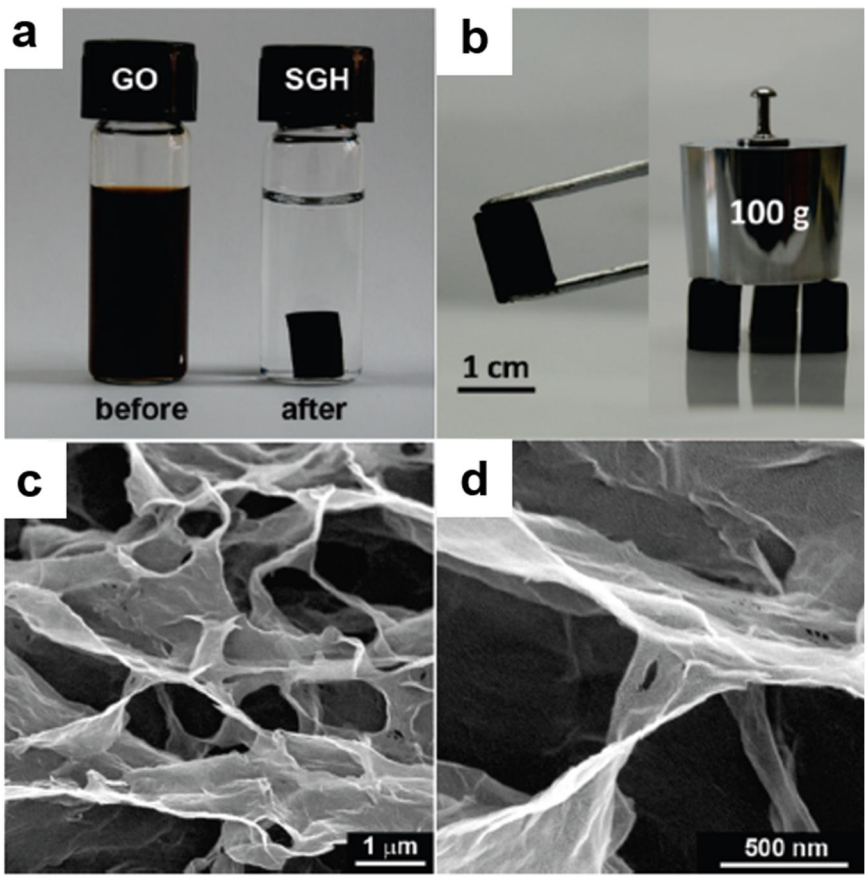

Figure 3-1. (a) Images of GO solution and hydrogel before and after hydrothermal method. (b) Image of strong hydrogel. (c-d) SEM images of different magnifications of the interior microstructure.

A conceptual diagram of the hydrothermal method can be found in figure 3-2. Fill the jarmed vessel with the GO solution dispersed in water. The cooked container is heated to 100℃ or higher. The heated water fills the empty space of the enclosed vessel with saturated vapor. The required amount of water evaporates at a pressure determined at a specific temperature. Because only a portion of the water filled in the vessel participates in the evaporation, the remaining water does not evaporate and becomes superheated water. The water is self-ionized.

In water below 100 ℃, one minute of water molecules dissociate and exist as H^+ and OH^- ions. However, the dissociation level in water which does not evaporate at a temperature of 100℃ or more increases, and the ion concentration increases. The concentration of the increased ion is about 100 times that of the normal pressure state.

As the ion concentration increases, the amount of H^+ ions in the water increases and the GO is reduced by H^+ ions. Reduced GOs lose their hydrophilic properties and condense to each other. The closer the graphene

is, the more the functional group of the GO reacts. This reaction is a dehydration in which the functional group reacts to escape the water molecule and to form a covalent bond between the functional groups.

It can be seen in Figure 3-3 (a) that the GO is reduced as the concentration of H^+ ions increases. In Figure 3-3 (b), the binding between graphene by dehydration can be confirmed [91-93].

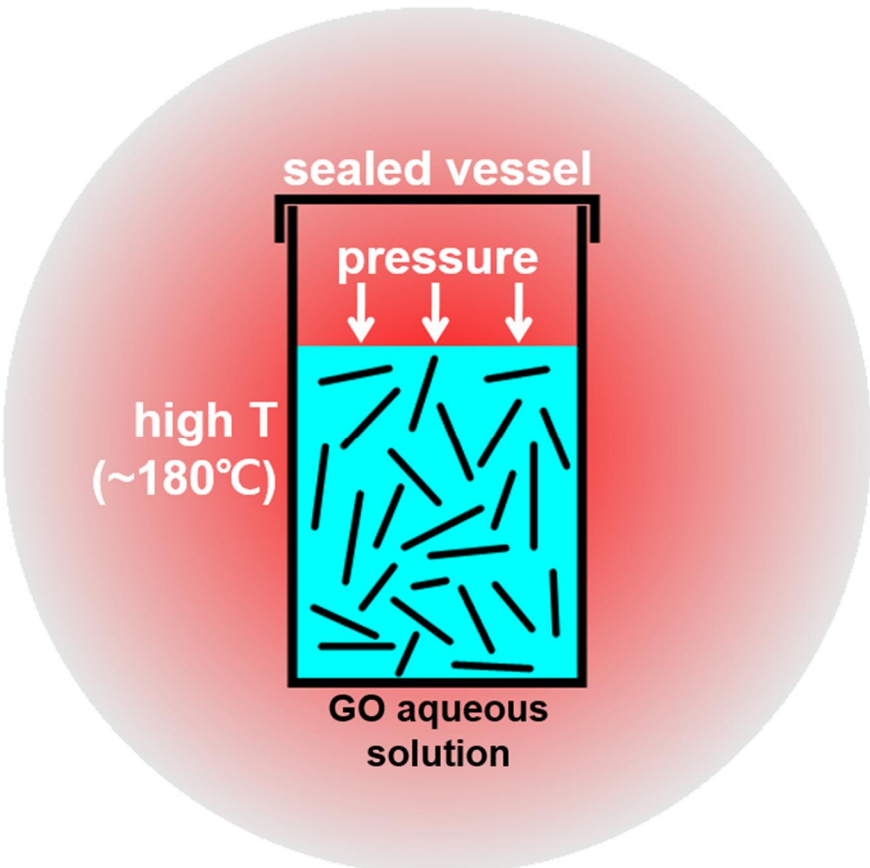

Figure 3-2. Schematic of hydrothermal method.

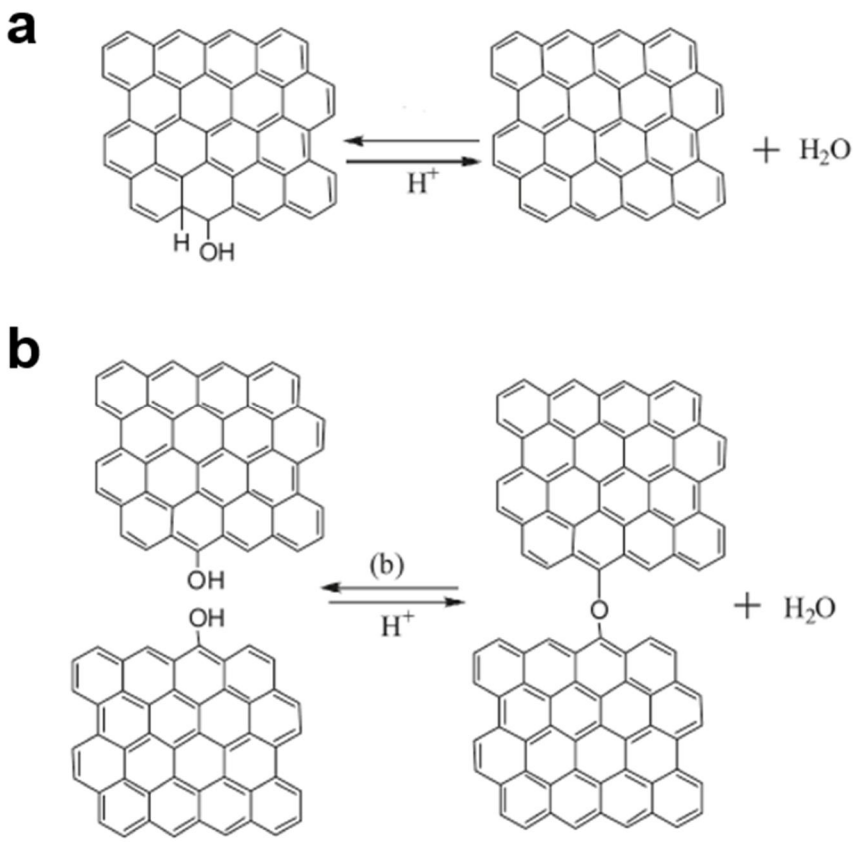

Figure 3-3. (a) Reduction of GO on hydrothermal method. (b) Dehydration reaction between graphene on hydrothermal method.

When heated in a sealed container to 180℃, the water does not evaporate and maintains the liquid state (figure 3-4). The GO dispersed in water increases the dissociation concentration of water and reduces it, leading to the binding of GO. The movement of the GO is not seen until around 160℃. However, we can confirm that graphene binds as the GO moves in water from 165℃.

From the bottom of the solution, as the graphene moves up, the concentration goes up and the chemical bond becomes visible in the picture. When the temperature reached 180℃, the movement of GO was not recognized. However, it was found that the chemical bond was induced in the structure after forming the structure [94].

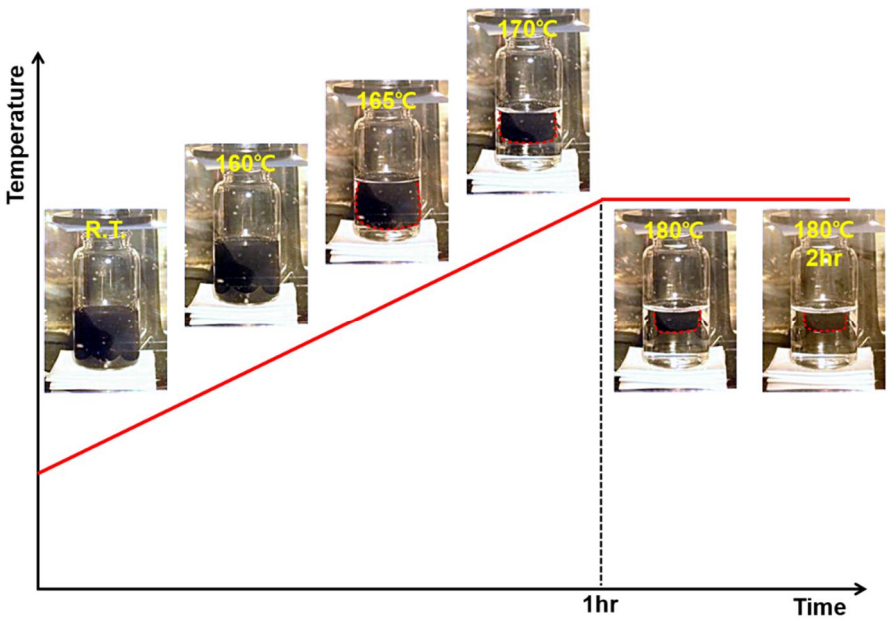

Figure 3-4. Fabrication of graphene hydrogel.

The conventional hydrothermal method uses a steel container capable of withstanding high pressure. Also, since the superheated water has high reactivity, the inner container is used as the fluorine material. This type of container can be excellent in safety, but it can't be confirmed that the actual graphene moves in the container. Therefore, our laboratory conducted a hydrothermal process using a glass vessel. Because it is a transparent glass material, it has the advantage of showing inside the container. Also. Both sides of the glass container were restrained using a Teflon film. A glass vise was used to seal the glass container with Teflon film (figure 3-5). The design was optimized by using the thermal expansion coefficients of glass, Teflon and steel. Through this design, real-time observations that were not confirmed in the existing literature were possible. We confirmed the movements of the GO by detecting the movements of the GOs in real time and reaching almost 180℃.

Figure 3-5 (b) shows the experimental set-up actually produced. The thickness of the Teflon film was set, and the thickness of the Teflon film to be placed on both sides of the glass container was determined, and a

reproducible experiment was conducted. Also, the shape of the glass vessel and the pressure of vise were designed and optimized to withstand the high pressure at which saturated vapor is generated at high temperature [95-99].

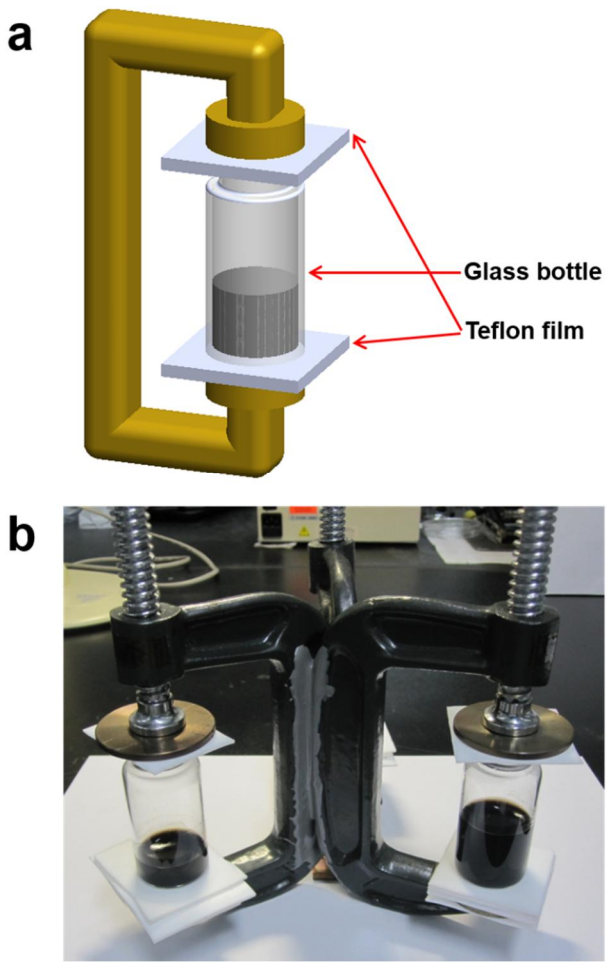

Figure 3-5. (a) Schematic of the experimental set-up. (b) Photograph of set-up.

Water having a boiling point of 100℃ has a property of maintaining saturation within a certain volume. If you limit the volume, only a certain amount of water evaporates. The water that does not evaporate is in a liquid state, and evaporation and condensation occur by vapor and water. There is no change in the mass of water and steam in one system because the amount of water evaporating and the amount of condensing steam are the same. If the volume is set to infinity, all water will evaporate to vapor at temperatures above 100℃. However, the amount of water that can be evaporated is fixed in a certain volume, and the pressure generated by the evaporated steam is also determined. This can be seen in the graph in figure 3-6.

The pressure of saturated vapor increases rapidly at temperatures above 100℃ and at saturated pressure of 10 bar at 180℃. This is a high pressure equivalent to 10 times the normal pressure. As the water evaporates in the sealed vessel, the pressure of 10 bar is applied to the vessel and the water which can't evaporate anymore becomes superheated water, which is involved in the reduction of GO and generation of graphene-based hydrogel.

This shows that it is important to design an experiment that can withstand high pressures while still allowing corrosion by high concentrations of ions.

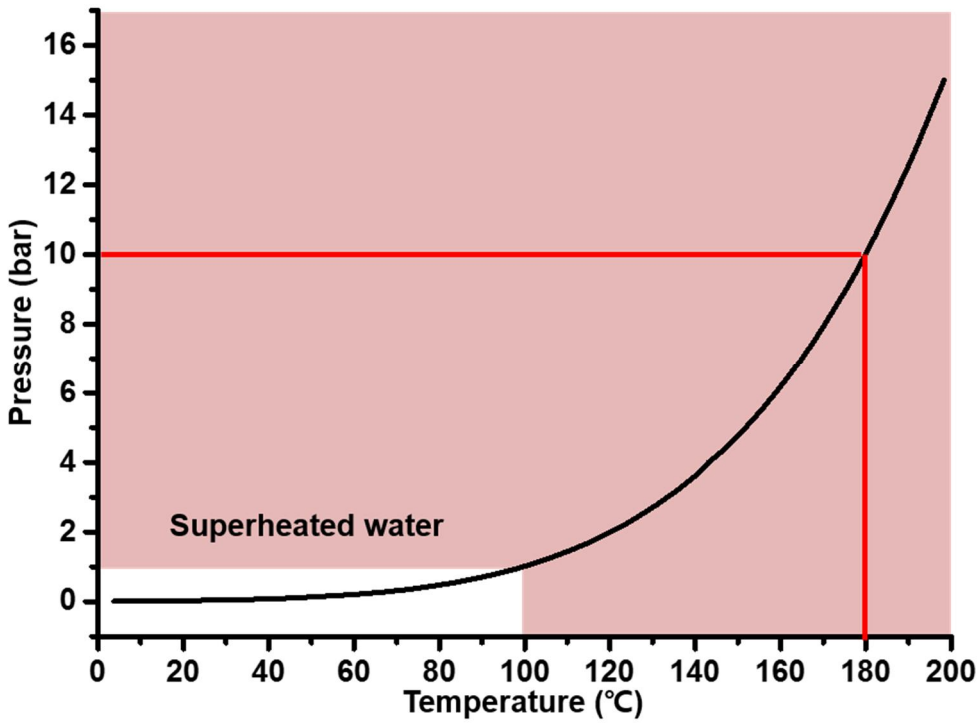

Figure 3-6. Relationship between temperature and pressure of saturated vapor.

3.1.2. Graphene-reduction agent hydrogel

As described in the previous chapter, existing hydrothermal processes require high pressure conditions at 180℃. This is because, as shown in figure 3-4, binding of graphene is induced at the same time as reduction at 165℃ or higher. When the GO dispersed in water is reduced, the physical property changes from hydrophilic to hydrophobic, and the dispersion degree in water is lowered. As a result, the graphene is assembled to form a structure.

However, the high temperature of 180℃ has the disadvantage that it has limit of experiment set-up. At 180℃, the pressure of saturated vapor is 10 bar and high pressure corresponding to 10 times of normal pressure is generated, and high reactivity of superheated water can cause corrosion of container.

Therefore, many researchers are working on the research to lower the temperature of the hydrothermal process. Since the graphene-based structure

starts from the reduction of GO, studies using an agent capable of promoting reduction have been led [100-104].

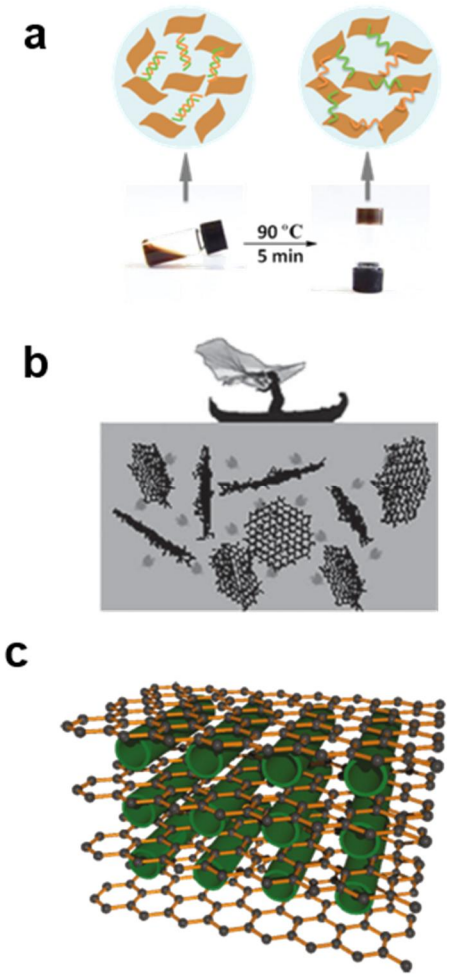

Figure 3-7. Reduction agent of (a) dsDNA. (b) Metal nanoparticle. (c) Carbon nanotube.

By controlling the degree of reduction of the GO, the temperature of the process can be lowered. We use a different approach from the conventional method, in which the functional group on the surface of the GO is reduced and desorbed to bond with adjacent graphene. Even if the reduction does not occur completely at low temperature, it induces the binding of graphene using an agent.

For example, using dsDNA, a structure can be fabricated at a relatively low temperature of 90℃. This is lower than the boiling point of water, but it is possible to form a structure because dsDNA acting as an agent assists graphene binding. Also, using divalent ion, ion penetrates between graphene and connects graphene. This can achieve binding of graphene regardless of the degree of reduction of GO. In addition, studies are underway to fabricate structures using carbon nanotubes. This has the advantage that various applications can be secured because the structure increases the porosity [105-108].

3.2. CVHT process

3.2.1. Need for graphitic film

Free-standing thin films are an integral part of portable and wearable devices, including electronic, optical, and mechanical devices, as well as energy storage devices. Because of the outstanding physical properties of graphene, considerable efforts have been made to produce graphene-based thin films or papers [109-110].

These thin films of graphene are invariably derived from graphene oxide (GO) nanoparticles, because of the ease and economy with which the films can be made, which are in turn reduced. The properties of the reduced graphene oxide (rGO), however, are nowhere close to those of graphene. It is highly desirable, therefore, to fabricate rGO thin films whose mechanical and electrical properties are fairly close to those of graphene.

Of various processes used to reduce GO, hydrothermal reduction is quite attractive because of its benign and green nature of the process, requiring

only water and a temperature around 200^{o}C for the reduction. In this hydrothermal process, neighboring GO nanosheets are reduced in an atmosphere of superheated water and they interact randomly and irregularly, resulting in a porous structure composed of partially reduced GO nanoplatelets. The graphene structure produced, therefore, has poor mechanical and electrical properties compared to those of graphene.

In this work, we introduce a 'confined vapor-phase' hydrothermal (CVHT) process for the fabrication of free-standing ultrathin rGO film or graphene film. In this process, a drop of GO solution is initially placed between two glass plates and the amount of water in the solution is set to be just sufficient to provide supersaturated vapor pressure upon evaporation at the desired temperature. Because of the pressure exerted by the supersaturated vapor on the glass plate and the directional escape of evaporated water along the plate plane, directional stacking and bonding occurs among GO nanoplatelets that are confined by the glass plates. The electrical conductivity of the film thus produced can be made as good as that of chemical-vapor deposited (CVD) graphene film [111-115].

3.2.2. New set-up for CVHT process

Figure 1 illustrates the procedure involved in the fabrication of rGO film or graphene film by CVHT process. The GO solution used in the experiment was prepared by a modified Hummer's method (graphite: BayCarbon, SP-1). The nanoplatelets of GO thus prepared are typically 1 μm long and about 1 nm thick with XPS confirming the formation of GO from the graphite.

Typically, 0.1 ml of GO solution is placed on a 1 cm by 1 cm glass plate, as shown in the first part of Figure 3-8(a), where the top and side views are given. The droplet formed on the plate spreads instantaneously due to capillary effect, covering the whole glass surface, when an upper glass plate is placed onto the lower plate (second part of Figure 3-8(a)). Subsequently, the sample confined by the two plates is placed in an autoclave specifically designed to have a volume of 25 ml (see Figure 3-8(b)) and it is heated for 3 hours at 180^{o}C. This volume yields a saturation pressure of about 10 bar when 0.1 ml of water is fully evaporated at 180^{o}C. Neither water nor GO solution is added to the autoclave.

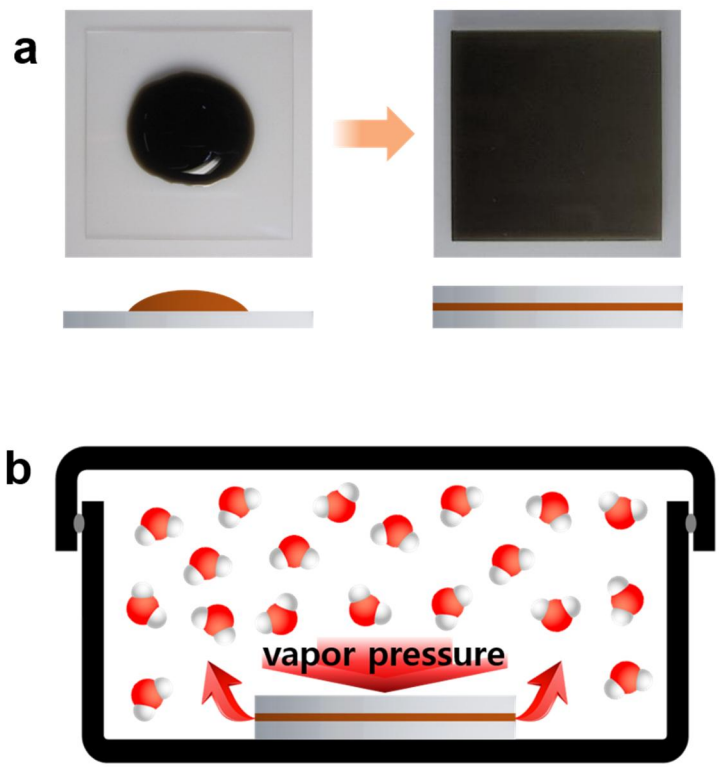

Figrure 3-8. (a) Top (optical images) and side (schematics in blue) views of prepared sample. GO solution is confined between two glass plates by capillary effect. (b) Schematic illustration of ‘confined vapor-phase’ hydrothermal process.

During the hydrothermal process, the high temperature over the boiling point of water causes transformation of water in the GO solution to superheated vapor and raises the vessel pressure. Initially, the GO nanoplatelets in the GO solution between the glass plates are randomly dispersed. As the water vapor escapes along the plane direction of the glass plates and the pressure is exerted on the glass plates, GO platelets tend to stack up directionally and the neighboring platelets are chemically combined by dehydration reaction and π-π interaction (see Figure 3-9(a)).

A free-standing graphene film prepared by CVHT method is shown in the upper part of Figure 3-9(b). The free-standing graphene film 100 nm thin that results from the process can be picked up and held upright with tweezers, as shown in the lower part of Figure 3-9(b). As apparent from the figure, the original shape is maintained at the end of the processing without transformation or shrinkage. With the usual hydrothermal method, in contrast, a three dimensional structure of graphene hydrogel is fabricated and more than 90 percent of volume fraction is water. To maintain the shape of the graphene structure, therefore, freeze-drying method is used. When the

graphene structure is dried in air, pores in the graphene structure shrink due to capillary force of evaporating water and the shape of the graphene structure is destroyed. The hydrothermal graphene film (HGF) fabricated by CVHT process can easily be removed from the plates because the film has been turned into a hydrophobic film by the reduction.

Scanning electron microscopy (SEM) images of the film are given in Figure 3-9(c). The images show that the surface of the film is smooth and no pores or cracks are present. Atomic force microscopy (AFM) was also utilized to assess the film thickness and its profile (see Figure 3-10). The image in the figure shows that the thickness is around 100 nm and that the thickness is rather uniform across the basal plane of the film. There have been recent reports on free-standing GO-based papers or films, and the thinnest free-standing film so far has been around 500 nm. Formation of a film consisting of highly aligned, stacked and densified GO platelets renders the film to stand freely even at the thickness of 100 nm.

Graphene oxide is synthesized from purified natural graphite (SP-1, Bay

Carbon) by the Hummers method. Colloidal dispersion of GO nanoplatelets in water at the concentration from 0.5 mg/ml to 5 mg/ml is prepared utilizing a sonicator. A glass wafer (Dasom RMS Co.) cleaned by SPM (sulfuric-peroxide mixture, H_2SO_4:H_2O_2 4:1) is diced into 1 cm by 1 cm pieces. A 0.1ml of GO solution trapped between two glass plates is placed in an autoclave which has a volume of 25 ml. It is then heated for 3 hours at 180^{o}C, which produces HGF between the two glass plates. Free-standing HGF can easily be peeled off the glass by submerging the sample into water. TGF can be prepared by annealing the HGF at 1,000^{o}C for 1 hour after reaching the temperature at a ramping rate of 5 ℃/min under vacuum with gas feed rates of 30 sccm for Ar and 15 sccm for H_2.

The structure of HGF is characterized by field-emission scanning electron microscopy (S-4800, Hitachi) and atomic force microscopy (XE-150, PSIA). For the measurement of the thickness of HGF, the free-standing HGF is placed on the surface of a cleaned Si wafer wetted by a drop of ethanol. Uniaxial tensile tests are conducted with a dynamic mechanical analysis (2980 DMA, TA Instruments). Clamps grip the separated two copper plates

to which the HGF or TGF film is bonded by epoxy. All tensile tests are conducted with a ramp rate of 1 mm/min and a clamp compliance of about 0.2 μm/N. The electrical conductivities of HGF and TGF are calculated from the sheet resistance measured by 4 point probe (FPP-5000, Miller) and the sample thickness obtained from AFM measurement. The interlayer spacing for HGF and TGF is determined by XRD spectroscopy (D8-Advance, Bruker Miller Co.). The elemental contents of HGF, TGF and graphite are obtained by elemental analysis (Flash EA 1112, Thermo Electron Co.).

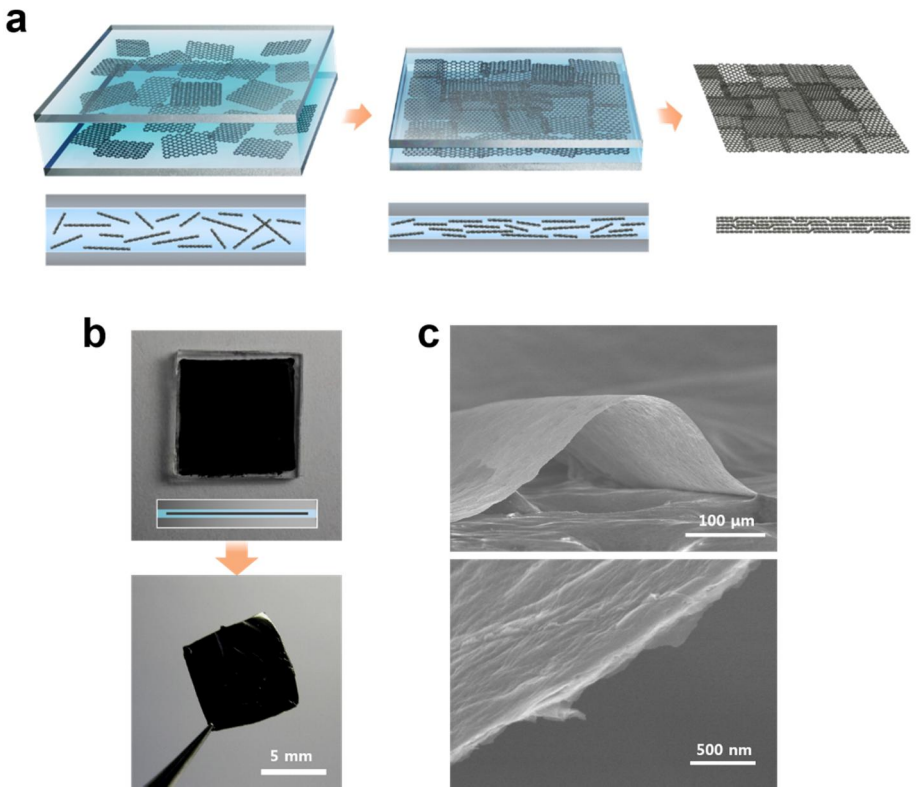

Figure 3-9. (a) Schematic illustration of the formation of graphene film during CVHT process. As the water vapor escapes along the plane direction of the glass plates and the pressure is exerted on the glass plates, GO nanoplatelets (rectangles in the upper row and the lines in the bottom row) tend to stack up directionally. (b) Optical images of fabricated HGF (side view illustration in blue). The free-standing HGF can be picked up and held

upright with tweezers. (c) SEM images of HGF. Bottom image is a magnified version of the top image.

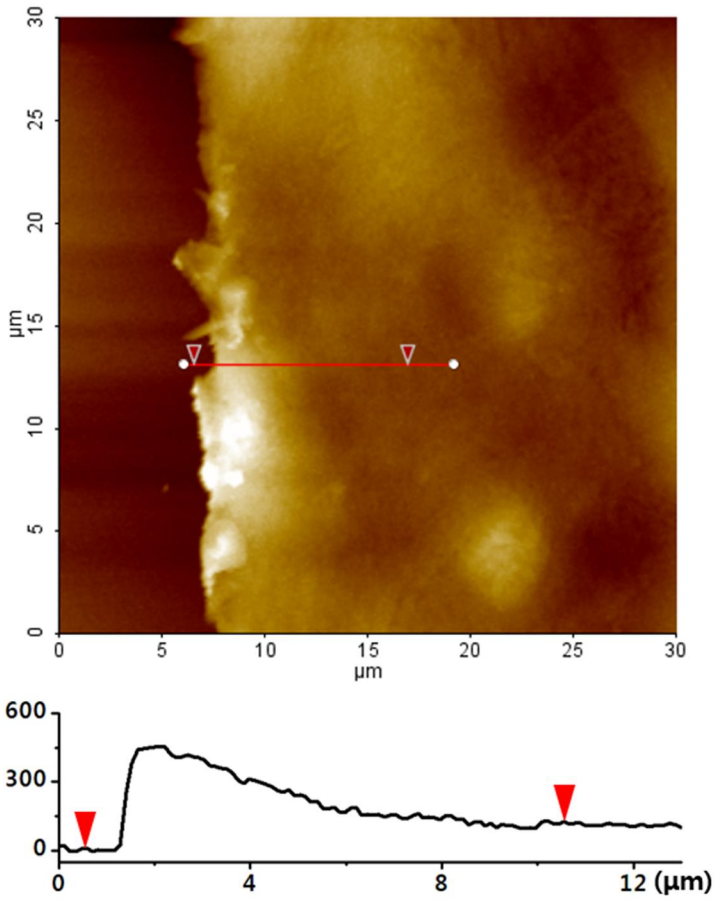

Figure 3-10. AFM image and thickness profile of HGF.

3.2.3. Thickness control of HGF

The transmittance of the film is of interest in the visible range, although a 100 nm thick rGO film would be too thick to be highly transparent. Figure 3-11 shows how transparent these films are when they are prepared with various concentrations of GO. In preparing the films, the volume of GO solution was fixed at 0.1 ml and the GO concentration was varied from 0.5 mg/ml to 5.0 mg/ml, expecting that a lower concentration would lead to a thinner film and thus a higher level of transparency. For the two samples corresponding to the concentrations of 0.5 and 1.0 mg/ml, the transmittance over the visible range was obtained with UV-visible spectrometer (see Figure 3-12(a)), revealing transmittance of 17 % and 26 %, respectively, at the wavelength of 550 nm. The film thickness as determined by AFM is plotted in Figure 3-12(b) as a function of the solution concentration. The plot shows that the thickness increases linearly with the concentration. The thinnest film prepared by CVHT process was 11 nm.

Thermal treatment is known to improve the properties of rGO film.

Therefore, HGF was reduced further by thermal annealing at 1,000^{o}C for 1 hour under vacuum with flows of Ar at 30 sccm and H_2 at 15 sccm. This thermally treated HGF is designated as thermally treated graphene film or TGF. As a result of the thermal reduction, the interlayer spacing was reduced from 3.81 Å for HGF to 3.40 Å for TGF, which is close to the spacing of graphite of 3.34 Å, according to the X-ray diffraction (XRD) spectroscopy result in Figure 3-13. The fact that TGF is much like graphite is also borne out in the elemental analysis result in Table 1. As shown, the oxygen content is 2.0 wt. %, which is perhaps the lowest oxygen content reported to date.

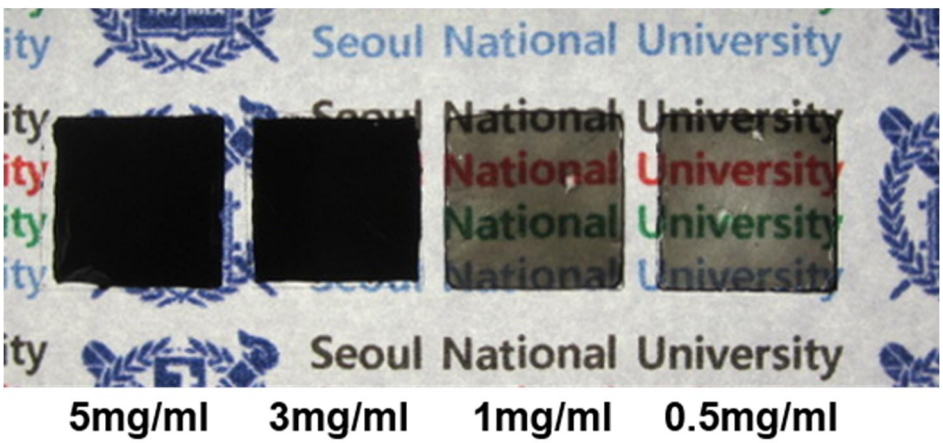

Figure 3-11. Optical images of HGF fabricated from various concentrations of GO solution. The film transmittance is proportional to its thickness.

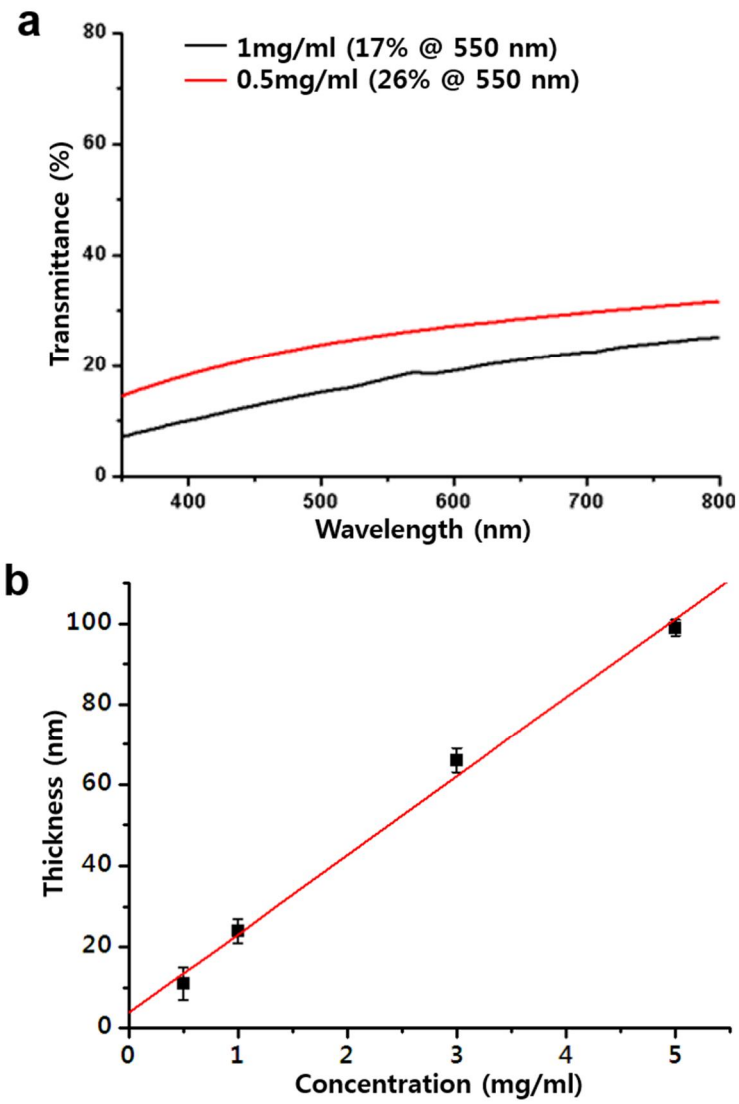

Figure 3-12. (a) Transmittance profile of HGFs. (b) Thickness of HGF as affected by concentration of GO solution.

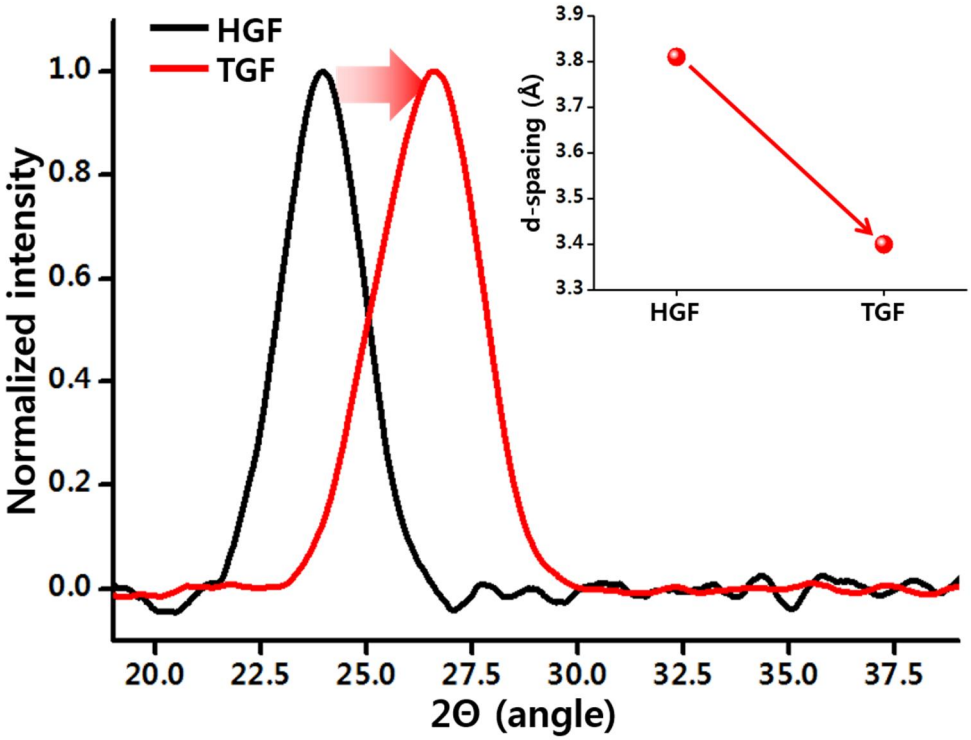

Figure 3-13. XRD data of HGF, TGF and the interlayer spacing of graphene film calculated from the XRD data.

Table 1. EA data in weight percent for HGF, TGF, and graphite (N: nitrogen, C: carbon, H: hydrogen, S: sulfur, O: oxygen).

	N	C	H	S	O	sum
HGF	**0.88**	**72.6**	**0.74**	**0.84**	**23.4**	**98.46**
TGF	**0.66**	**95.1**	**0.24**	**1**	**2.01**	**99.06**
graphite	**-**	**98.7**	**-**	**-**	**0.47**	**99.17**

3.2.4. Mechanical property of graphitic film

Papers of GO fabricated by vacuum filtration or spray coating are brittle and can easily buckle upon bending. For instance, the GO paper bent between two parallel plates buckled when the gap between the plates was 500 μm. Unlike GO platelets that are weakly bound in these papers, those in HGF are bound strongly by dehydration combination and π-π coupling. Therefore, HGF delivers a robust performance against bending and compression. As shown by the SEM images in Figure 3-14, no buckling took place even when the bending gap between the two plates was reduced down to 50 μm, and the film recovered to its original shape when released from the compression. The demonstration shown by the SEM images exemplifies highly strong and robust characteristics of the film that are yet to be matched. The robustness of HGF was also demonstrated in a sonication test. As shown in Figure 3-16, HGF maintained its original shape even after 5 hours of sonication.

A result of the reductive thermal annealing was an improvement in

mechanical properties, as shown in the dynamic mechanical analysis (DMA) results presented in Figure 3-15 for HGF and TGF. The measurement set-up is shown in the inset of the Figure 3-15. The stages holding the copper plates (refer to the inset) was moved at a rate of 1 mm/min and the force applied between the stages was measured. The stress-strain profiles thus obtained are given in Figure 3-15 for both HGF and TGF. The mechanical properties obtained for HGF and TGF are compared in Table 2 with those of the graphene films and papers reported in the literature. Notably, the Young's modulus (58 GPa) and tensile strength (1,399 MPa) of HGF are the highest reported ever for graphene films and papers even without any thermal treatment, as indicated by the figure and the values listed in Table 2. This high tensile strength is an indication that the GO nanoplatelets in the film are well aligned, tightly stacked, and strongly bound in the film. For the thermally treated HGF, or TGF, the values are 92 GPa and 1,743 MPa, respectively. The tensile strength of TGF of 1,743 MPa represents almost an order of magnitude increase in the strength over any reported so far for graphene films or papers. In fact, the graphene film is as strong as steel.

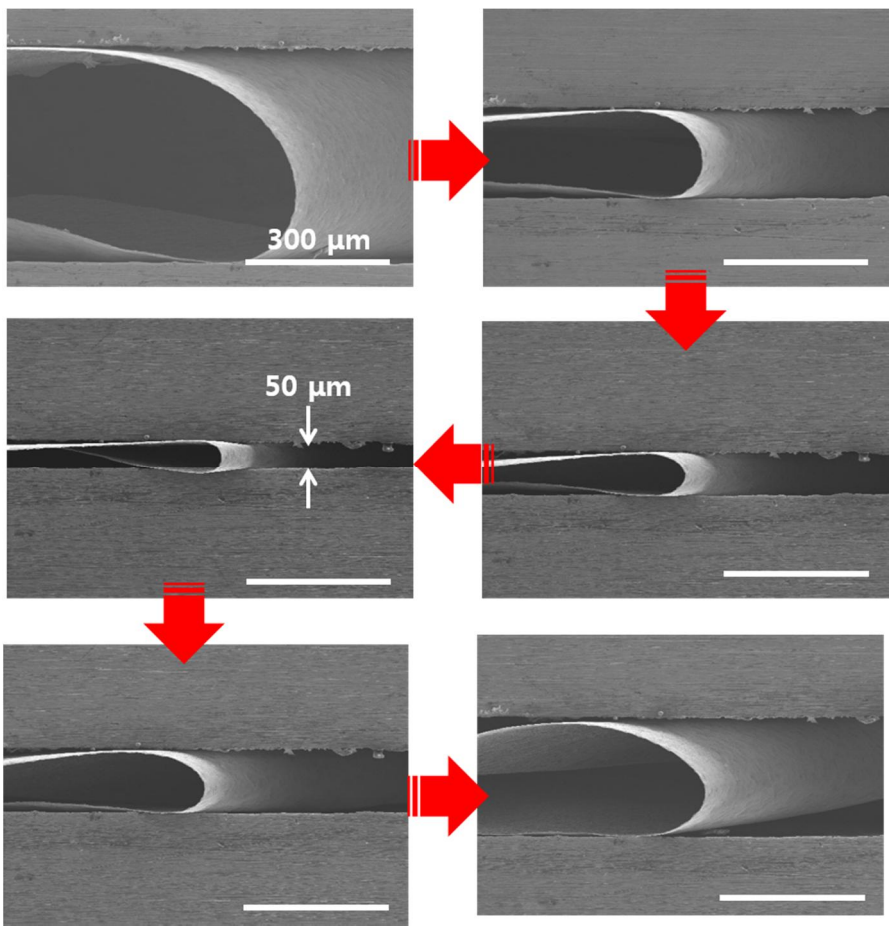

Figure 3-14. Bending gap of HGF can be rendered as small as 50 µm without causing buckling. The film returns to its original shape upon releasing the compression [116-118].

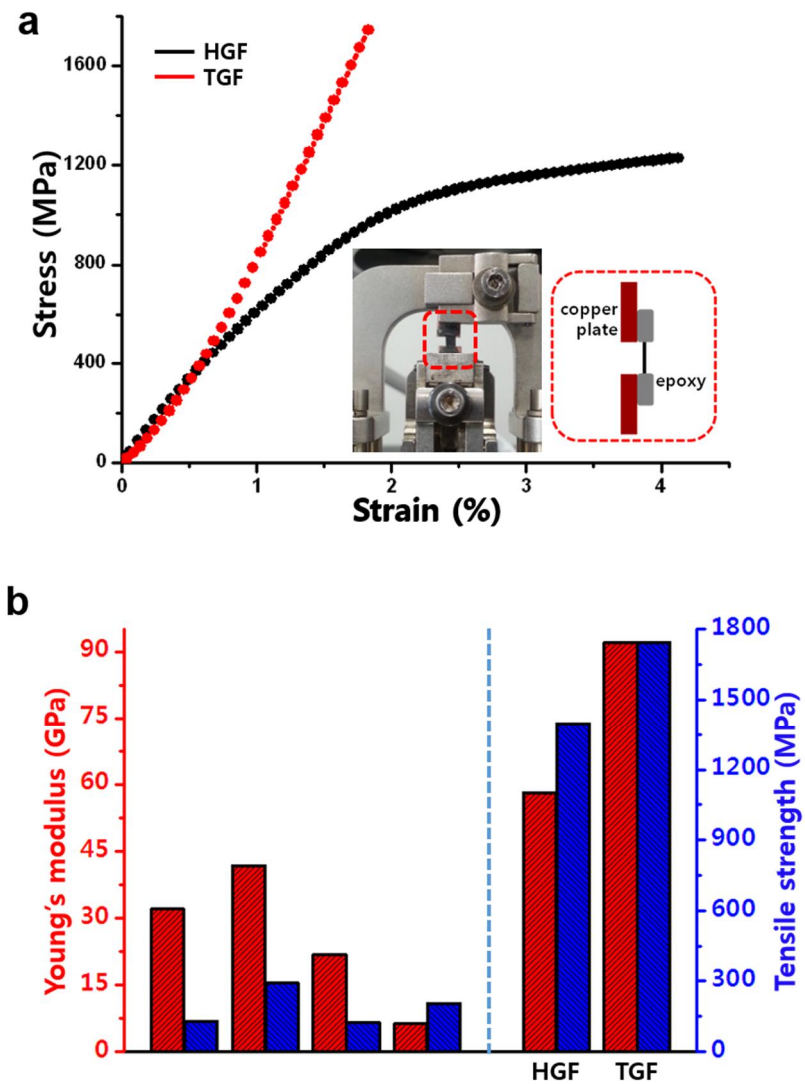

Figure 3-15. (a) Stress-strain curve of HGF and TGF. Inset shows the set-up for the measurement. (b) Comparison of mechanical properties of HGF and TGF with those reported in the literature for graphene films and papers.

Table 2. Mechanical properties of graphene films prepared by various methods.

	preparation method	Young's modulus (GPa)	tensile strength (MPa)
	graphene oxide	**32**	**130**
	annealed (220 ^{0}C)	**41.8**	**293.3**
	Ca^{2+} modified	**21.8**	**125.8**
	chitosan modified	**6.3**	**206**
HGF		**58**	**1399**
TGF	**annealed (1000 ^{0}C)**	**92**	**1743**

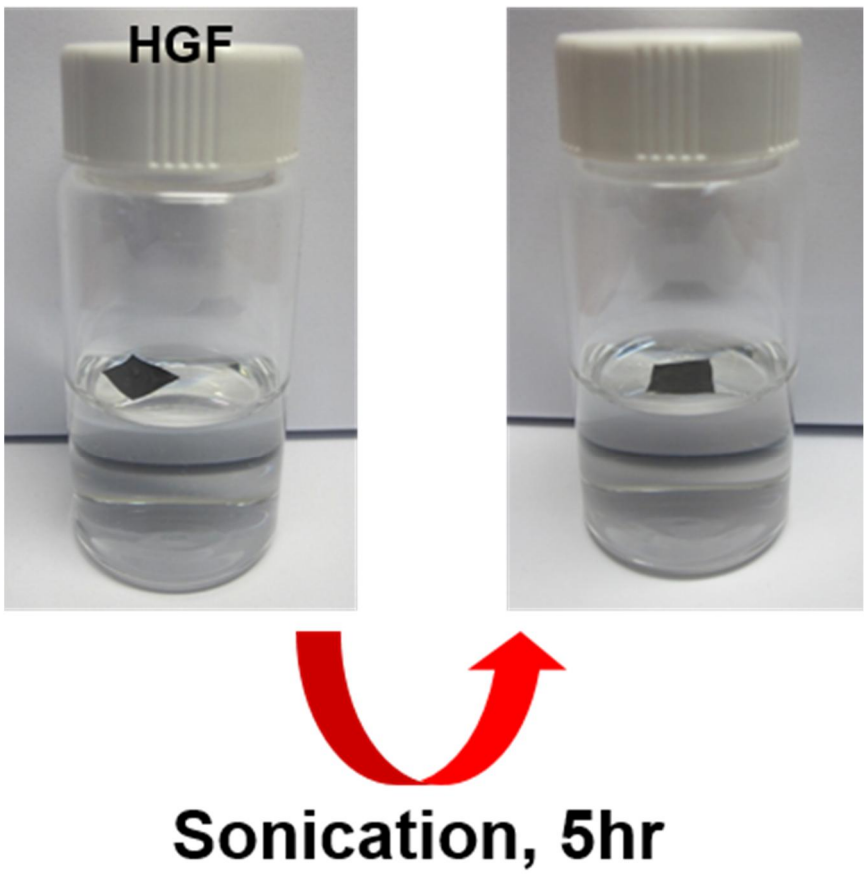

Figure 3-16. Unaltered graphene film of HGF after 5 hours' sonication.

3.2.5. Electrical property of graphitic film

A remarkable change in electrical conductivity results when HGF is reductively annealed to produce TGF. Figure 3-17 shows that the electrical conductivity is increased from 116 S/cm to 4,944 S/cm as HGF is thermally reduced to TGF, a nearly fiftyfold increase. This conductivity is the highest ever reported for graphene film or paper and represents almost an order of magnitude improvement in conductivity compared to the values reported for the usual graphene film or paper. Recrystallization of graphene film at approximately 2,000℃, on the other hand, resulted only in a conductivity of approximately 2,000 S/cm. Taken together, these results suggest that original configuration of nanoplatelets in graphene film or paper has more influence on electrical conductivity than recrystallization. Although nanoplatelets in HGF are well aligned and stacked, the oxygen content is still 23.4 wt. %, which explains the relatively low electrical conductivity in spite of well aligned and tightly packed nanoplatelets. With the reductive thermal annealing, the oxygen content is lowered to 2.01 wt% and a remarkable improvement in the conductivity results.

Confined vapor-phase hydrothermal process has been introduced for producing unusually robust graphene film, or HGF. This free-standing 100 nm thin film, which is as strong as steel, can be bent down to a bending gap of 50 μm before buckling and the bent film springs back to its original shape when released from the compression. The origin of this robustness lies in the alignment and packing of GO nanoplatelets induced by the CVHT process of forming the film. When this HGF is thermally reduced to form TGF, the electrical conductivity is increased from 116 S/cm to almost 5,000 S/cm, surpassing the conductivity of ordinary graphene papers by almost an order of magnitude and even surpassing the conductivity obtained by recrystallization at 2,000^{o}C. This graphene film with its outstanding properties should be valuable for portable and wearable devices, and other applications involving films for field emission, water treatment, gas barrier, lithium ion battery, and supercapacitor.

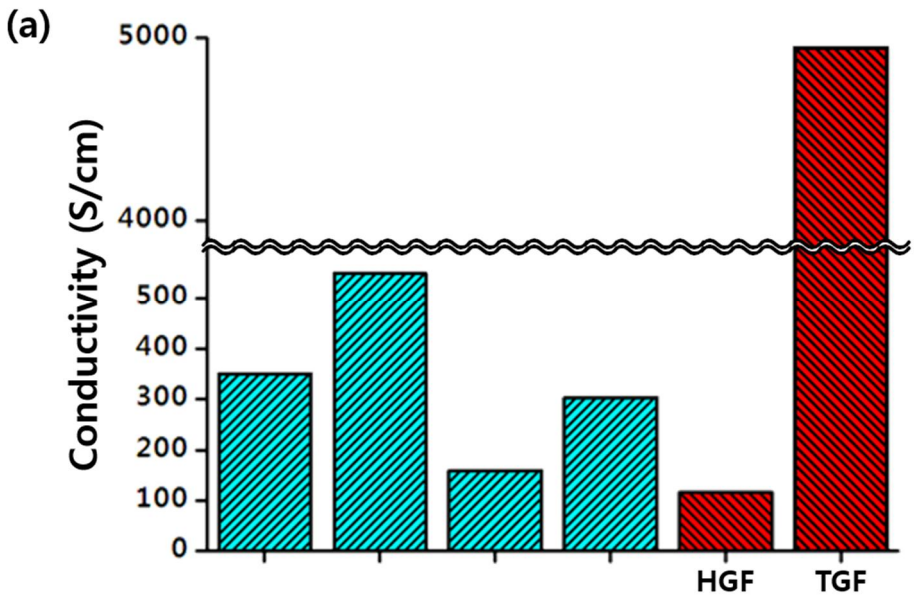

Figure 3-17. Comparison of electrical conductivity of HGF and TGF with that reported in the literature for various graphene films and papers [119-122].

Table 3. Preparation methods and the corresponding conductivities.

	preparation method	Conductivity (S/cm)
Ref 23	**annealed (500 ^{0}C)**	**351**
Ref 25	**annealed (1100 ^{0}C)**	**550**
Ref 17	**N_2H_4 - reduced**	**160**
Ref 22	**HI-$C_2H_4O_2$ - reduced**	**304**
HGF		**116**
TGF	**annealed (1000 ^{0}C)**	**4944**

Chapter 4. Gas separation property

Through the CVHT process mentioned in the previous chapter, a graphitic film with excellent physical properties was produced. This study was applied to gas separation. Most of the conventional gas separation membranes were polymer types. However, it has a trade-off relationship between permeance and selectivity. We will describe a membrane-based membrane fabrication technique and performance evaluation to overcome the disadvantages of polymer-based membranes.

4.1. Background of gas separation

4.1.1. Need for membrane

Membrane technology means selectively separating only the desired substances from a mixed gas or solution. The principle of separation uses various principles such as physical, chemical, and mechanical. Primarily, selective separation techniques using size differences of mixed materials are used (figure 4-1).

Such separation techniques have various applications. Wastewater produced by many factories contains a mixture of organic solvents and water. Since such wastewater is the main cause of environmental pollution, it is necessary to separate the harmful solution and water and to treat wastewater. In addition, oil spilled into the sea by accident causes serious marine pollution. In this case, the separation and recovery of the oil must be accompanied by a rapid recovery. The situation in which water and oil are separated from each other frequently occurs and it is a necessary skill to

maintain a clean environment. The largest category of membrane technology is the separation of water and oil.

As environmental pollution becomes serious, the amount of drinking water that people can drink is decreasing. The development of new drinking water production technology is imminent due to environmental disasters such as global warming. The technology of converting seawater into freshwater, which accounts for 97% of the Earth, is an essential technology not only for the present but also for the future. The technique to convert seawater to fresh water is to use the osmosis and reverse osmosis. Both methods use a filter that can remove salts dissolved in water. Therefore, it is necessary to develop high-performance membranes that can resist salt.

Most of the harmful gases generated from the power plant are composed of CO_2. CO_2 is the main cause of global warming and must be separated and captured in the atmosphere. Therefore, it is urgent to develop a membrane fabrication technology capable of separating only desired gases such as CO_2 from various gas molecules. Membrane fabrication technology using

various materials is available, but it is necessary to develop a new material membrane because of its limitations [123-126].

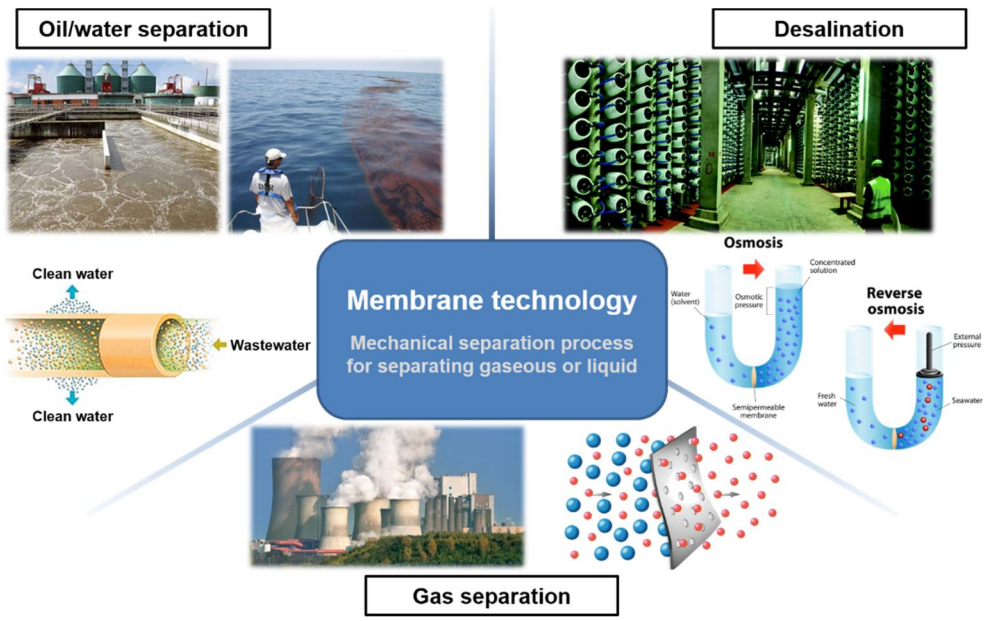

Figure 4-1. Various applications using membrane technology.

4.1.2. CO_2/N_2 and CO_2/CH_4 separation

To mitigate global climate change, an economical way of separating carbon dioxide from flue gas has to be found, which accounts for 40% of all carbon dioxide emissions. Membrane separation could be a viable solution, provided the carbon dioxide flow rate through the membrane is larger than 1,000 GPU (gas permeation unit in 10^{-6} $cm^3/cm^2/cmHg/s$) with a selectivity higher than 20 with respect to nitrogen. However, there is a tradeoff between permeance (volumetric flow rate) and selectivity. Moreover, the usual angstrom size pores with molecular selectivity are not favorable for high throughput. Here we show that graphitic membranes synthesized directly from graphene oxide nanosheets deliver a permeance of 8,000 GPU at a selectivity of 20. The selectivity can be increased to 58 with little loss of permeance by carbonizing the synthesized membrane film.

Unlike the usual hole-like pores, molecules pass through the slit channels in the graphitic structure. The molecular selectivity is achieved by the height of the channels and the high flow rate is allowed by the relatively huge width

of the channels, the aspect ratio being of the order of 10,000. Unlike the usual sorption-diffusion through molecular sieves, one molecular layer movement of molecules through the slit channels exhibits the characteristics of Hagen-Poisseuile law that governs bulk laminar flow. In contrast to the polymer membranes incorporating metal organic framework (MOF) that are sensitive to a change in pressure and the zeolite membranes sensitive to temperature, the graphitic membranes are insensitive to these changes, and to time of use. The high permeance realized here with slit channel pores suggests that tailoring pore structure could be essential for overcoming the problem of low permeance that is inherent to the circular pores with molecular selectivity or size in the range between 3 and 7 angstroms. The synthesized membranes are also effective in terms of permeance and selectivity for the separation of carbon dioxide from natural gas and bio-gas [127-129].

4.2. Fabrication of graphitic membrane

4.2.1. Properties of graphitic film

During the hydrothermal process, the high temperature over the boiling point of water causes transformation of water in the GO solution to superheated vapor and raises the vessel pressure. Initially, the GO nanosheets in the GO solution between the glass plates are randomly dispersed as schematically illustrated in figure. Because of the pressure exerted by the supersaturated vapor on the glass plates and the directional escape of evaporated water along the plate plane, directional stacking and bonding can occur among the confined GO nanosheets. The neighboring nanosheets are chemically combined by dehydration reaction and π-π interaction during the synthesis.

A free-standing graphitic film 100 nm thick prepared by the CVHT method was subjected to a bending test as shown in figure. There have been recent reports on free-standing GO-based papers or films, and the thinnest free-

standing film so far has been around 500 nm. Formation of a film consisting of highly aligned, stacked, and densified GO sheets renders the film to stand freely even down to the thickness of 60 nm. Papers of GO fabricated by vacuum filtration or spray coating are brittle and can easily buckle upon bending. For instance, the GO paper bent between two parallel plates buckled when the gap between the plates was 500 μm. Unlike GO sheets that are weakly bound in these papers, those in HGF are bound strongly by dehydration reaction and π-π coupling. Therefore, HGF delivers a robust performance against bending and compression. As shown by the scanning electron microscopy (SEM) images in figure, no buckling took place even when the bending gap was reduced down to 50 μm, and the film recovered to its original shape when released from the compression. The demonstration shown by the SEM images exemplifies highly strong and robust characteristics of the film that are yet to be matched.

The film thickness as determined by SEM and atomic force microscopy (AFM) (figure 4-3) is plotted in figure 4-4 as a function of the concentration of the GO solution. The figure shows that the thickness

increases linearly with increasing concentration. The thinnest film prepared by the CVHT process was 5 nm.

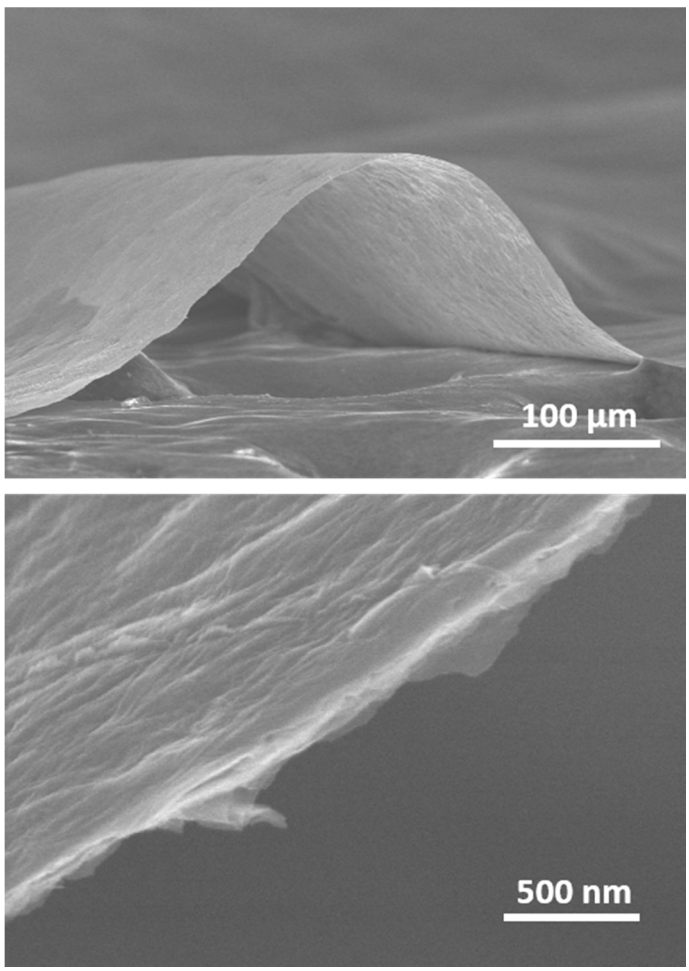

Figure 4-2. SEM images of HGF that is 100 nm thick. It is confirmed that HGF has smooth surface and flexibility.

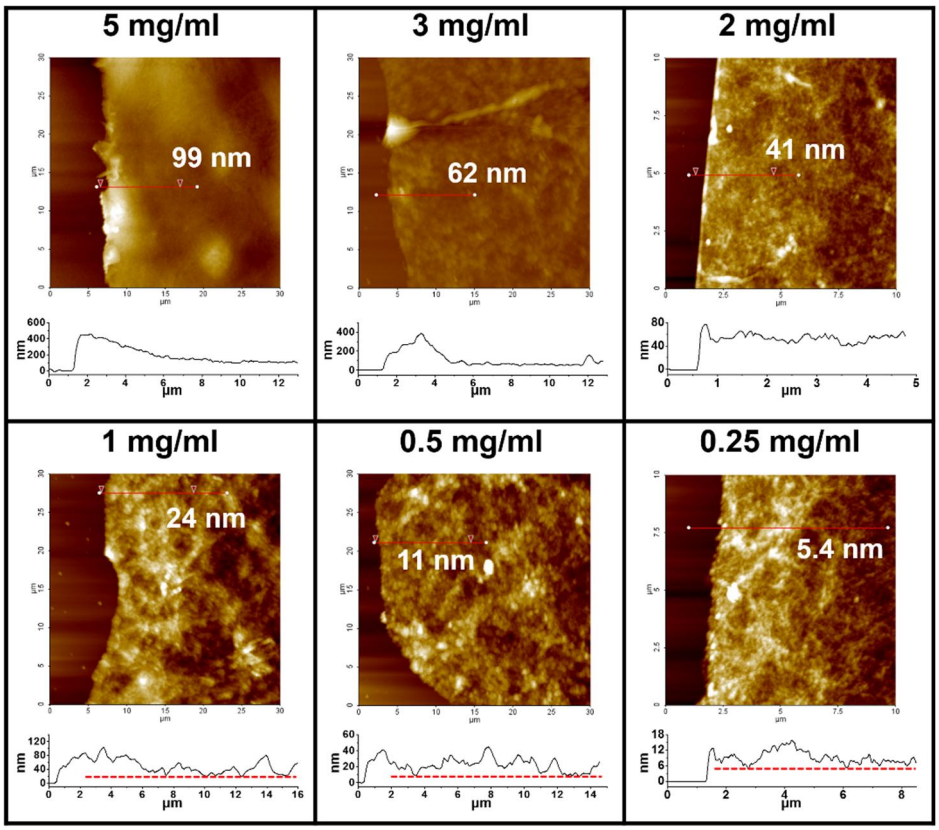

Figure 4-3. Controllable thicknesses of HGF as a function of the GO solution concentration.

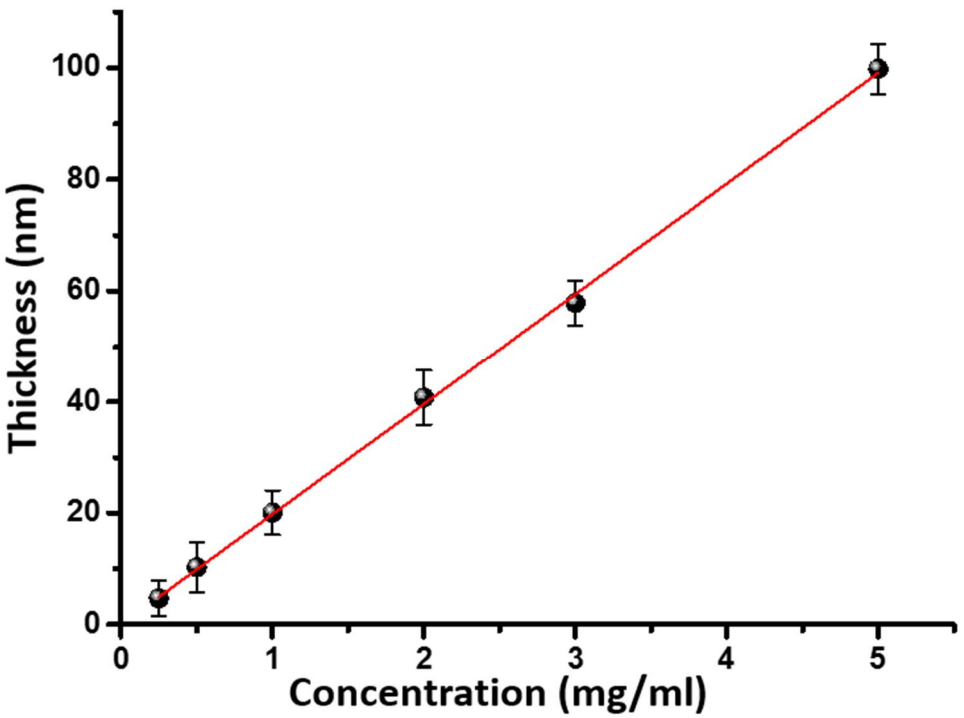

Figure 4-4. HGF thickness as determined by GO solution concentration.

4.2.2. XRD data of graphitic film

The superior alignment of the prepared graphitic films was confirmed by XRD data (figure 4-5). D-spacing was controlled through heat treatment to improve gas separation performance. The film heat-treated at 1000℃ was named TGF1, and the film heat-treated at 2200℃ was named TGF2.

It was confirmed that the d-spacing decreased as the heat treatment temperature increased. HGF has a d-spacing of 4 Å, whereas TGF1 has a d-spacing of 3.5 Å and TGF2 has a d-spacing of 3.4 Å. This is close to the d-spacing of pure graphite 3.34 Å (figure 4-5).

In addition, the good alignment of the graphitic film can be confirmed by the interval of the XRD peaks. As the annealing temperature increases, the interval of the peaks decreases. This means that the d-spacing inside the film is uniform. The XRD peaks of GO have wide spacing (Figure 4-7). On the other hand, HGF has a relatively narrow spacing, which means that the spacing within the film is uniform. In other words, it means that the alignment of the graphene constituting the film is excellent.

Therefore, it can be said that as the heat treatment temperature is increased, the interval is reduced and the alignment property is improved.

Figure 4-6 shows that the graphitic film has uniform properties. The XRD data obtained at various points have not only a uniform peak shape but also a peak maximum value.

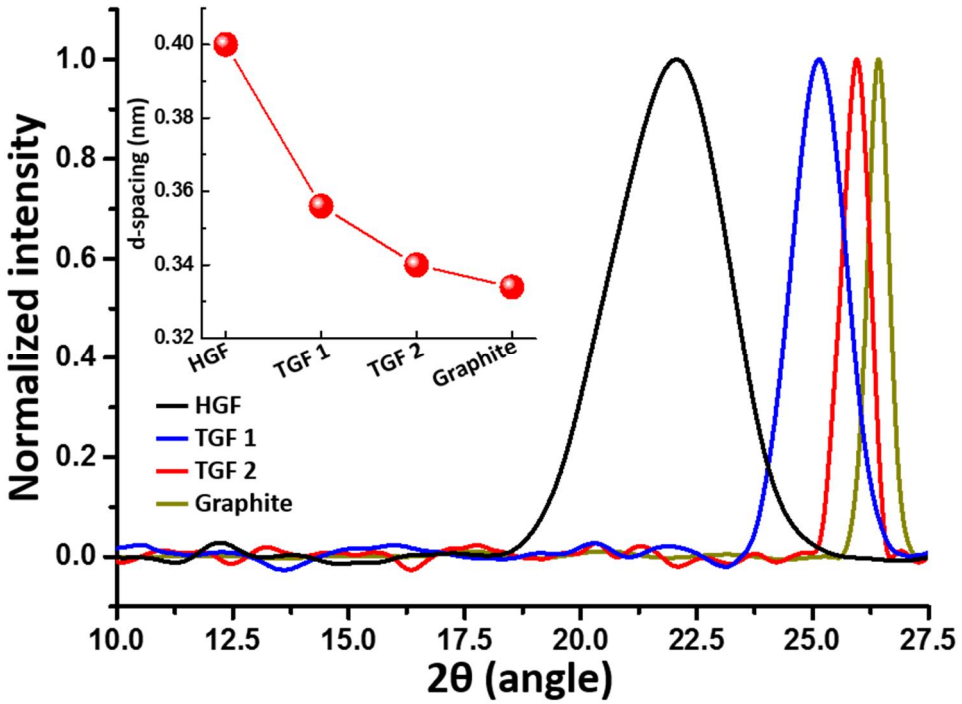

Figure 4-5. XRD peak profiles of HGF, TGF1, and TGF2, compared with that of graphite.

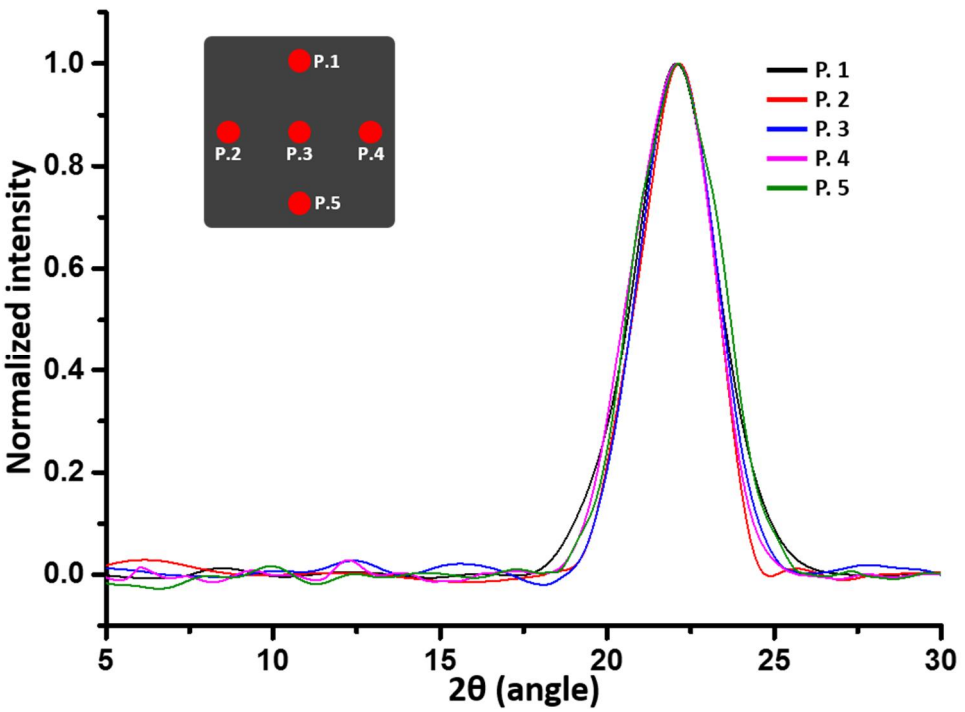

Figure 4-6. XRD profiles obtained at 5 different positions on HGF.

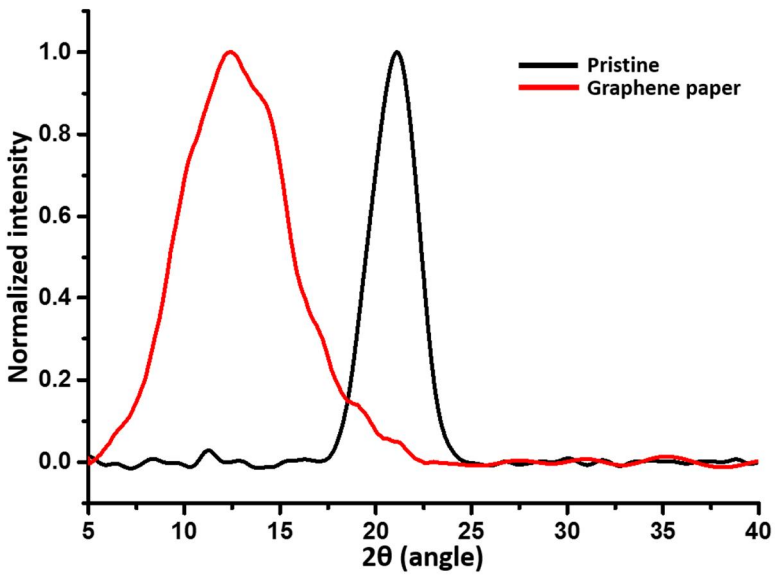

Figure 4-7. XRD peaks of graphene paper and HGF. The HGF peak is much sharper, indicating a better ordering of nanosheets.

4.2.3. Experimental set-up

In the gas separation experiments, gases of CO_2, N_2, O_2, and CH_4 were used. Membranes were fabricated as shown in figure 4-8 so that the gas could only pass through the graphitic film. It is necessary to ensure the rigidity of the graphitic film because the gas permeates at a pressure of 1 bar higher than the atmospheric pressure. Therefore, a porous polyethersulfone (PES) membrane was used as a supporting layer on both sides of the film. In order to allow the gas to pass through only the graphitic film, the edge of the film and the PES membrane are coated with an epoxy that can't permeate the gas.

The fabricated membrane was mounted on a filter holder and the permeance of the gas permeated through the graphitic film was measured using a bubble flow meter. The permeability of each gas was measured by measuring the velocity of the bubble inside the bubble flow meter.

The selectivity was calculated as the ratio of the measured gas permeance. The permeance was measured by using HGF, TGF1 and TGF2, and the

experiment was carried out for 6 different thicknesses ranging from 5 to 100 nm.

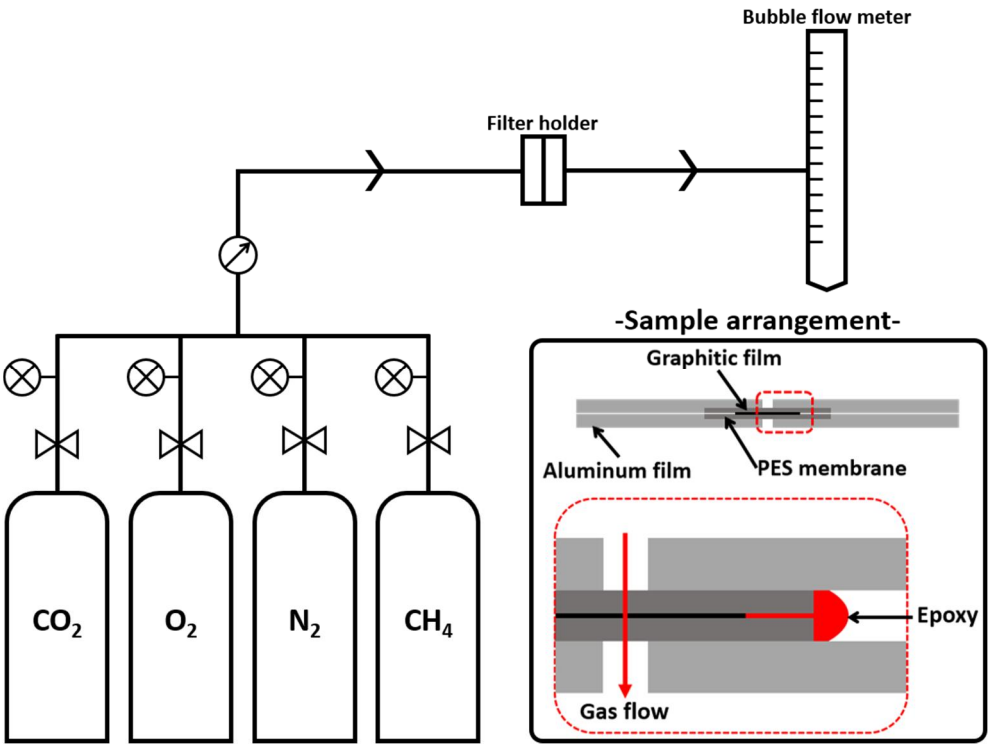

Figure 4-8. Schematic experimental set-up. Inset images show the fabricated gas separation membrane.

4.3. Gas separation performance

4.3.1. CO_2/N_2 separation

The selectivity attainable with the membranes for post-combustion carbon capture is generally known to suffer at high temperature. For instance, the selectivity of a polymeric membrane at 30°C, which is 36, decreases to 25 at the typical flue gas temperature of 50°C. Zeolite membrane is also temperature-sensitive. Figure 4-9(b) shows that the selectivity of the graphitic membrane is not affected at all by temperature, up to 80°C. This insensitivity to temperature also extends to permeance. As shown in the figure, the permeance stays almost the same despite the rise in temperature.

While the synthesized HGF has a good crystalline structure, a still better ordered structure should result upon carbonizing the HGF. The thermal treatment would cure the defects generated in the course of forming the hydrothermal HGF. For the purpose, the HGF was carbonized by thermal annealing at 1,000°C and also at 2,200°C for 1 hour with flows of

Ar (30 sccm) and H_2 (15 sccm). This carbonized HGF is designated as thermally treated graphitic film or TGF: TGF1 for the film treated at 1,000°C and TGF2 for the film treated at 2,200°C. As apparent from the XRD peaks in Supplementary Fig 8, the film becomes more graphitic as the film goes through thermal treatment at higher temperature. In fact, TGF2 is fairly close to graphite itself in terms of peak position and half-width at full maximum (HWFM). The interlayer spacing was reduced from 4.00 Å for HGF to 3.51 Å for TGF1 and to 3.40 Å for TGF2, which is close to the graphite spacing of 3.34 Å, as shown in the inset of the figure.

Figure 4-10 shows the permeance and the corresponding selectivity attainable with three different kinds of graphitic films studied here: hydrothermal HGF (black stars in the figure) and thermally treated HGF of TGF1 (blue stars) and TGF2 (red stars) for various film thicknesses ranging from 5 nm to 100 nm. An immediate observation is that the selectivity is substantially increased as a result of the thermal treatment with little loss of permeance. For instance, the CO_2/N_2 selectivity is increased from 20 (HGF) to 58 (TGF2) for the same 5 nm thickness with not much loss in permeance,

i.e., 8,000 GPU (HGF) vs. 7,000 GPU (TGF2).

Another observation is that only a small loss in selectivity results when the film thickness is decreased for higher permeance for the thermally treated film membranes. For the TGF2 membrane, for instance, the selectivity decreases from 63 to 58 when the thickness was reduced from 100 nm to 5 nm. As shown in figure 4-5, the peak width or HWFM, which is a measure of stacking faults, gets smaller as HGF is thermally treated more fully, indicating that the degree of stacking faults is lower for TGF1 than HGF, and still lower for TGF2 as a result of higher temperature annealing. Therefore, the selectivity is higher for more thermally treated film, TGF2 showing the highest selectivity and HGF the lowest for the same permeance.

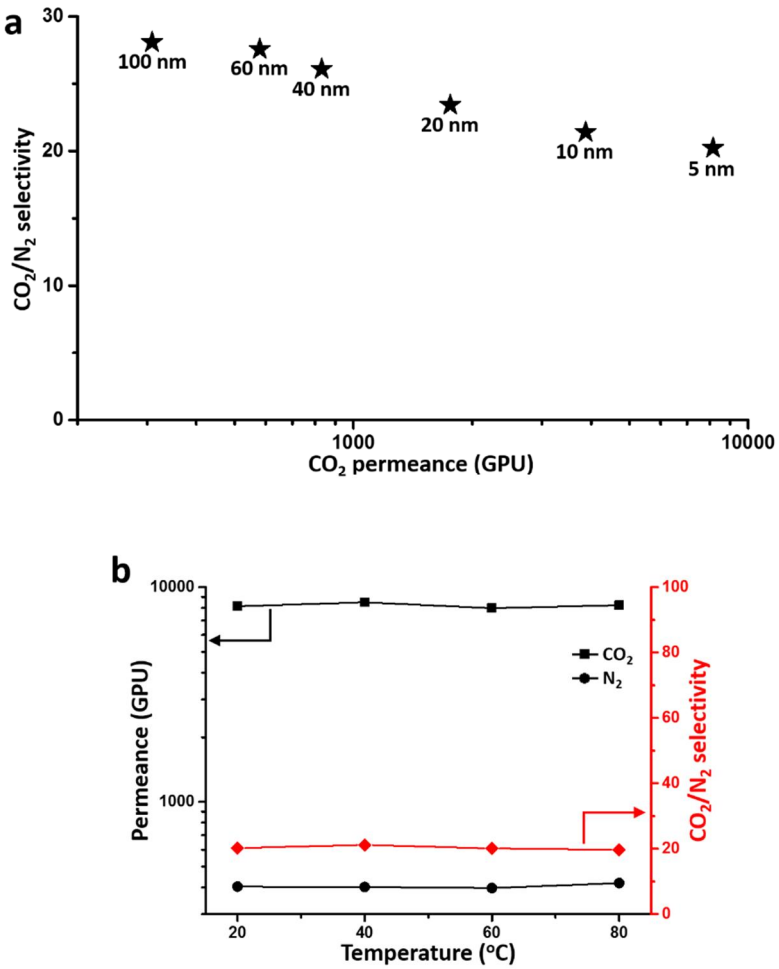

Figure 4-9. (a) CO_2 selectivity and permeance as affected by the film thickness ranging from 5 nm to 100 nm. (b) Temperature effect on permeance and selectivity of the HGF 5 nm thick, showing negligible influence.

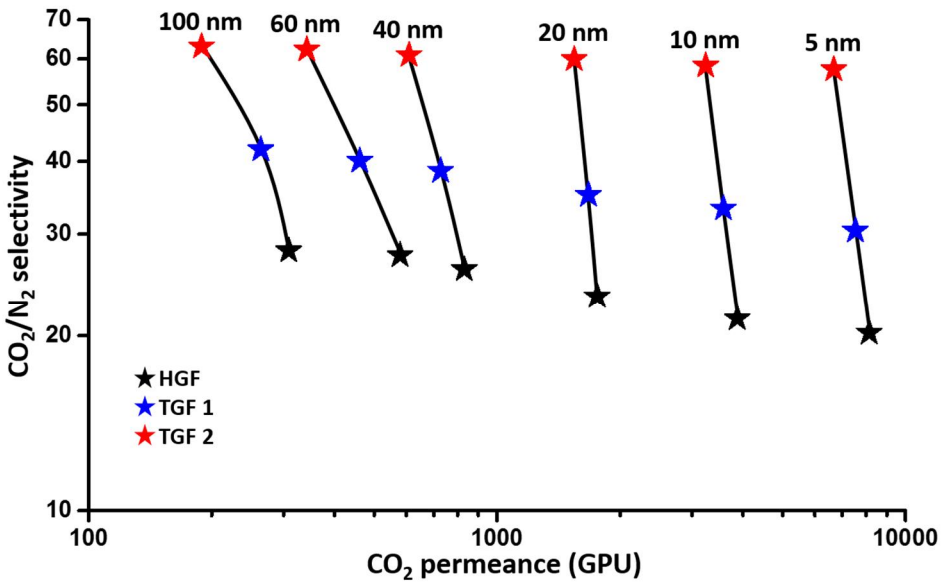

Figure 4-10. CO_2 selectivity vs. permeance for HGF (black stars), TGF1 (blue), and TGF2 (red) membranes for various film thicknesses ranging from 5 nm to 100 nm.

To investigate the behavior of the flow through the graphitic film membranes, the permeance of CO_2 through the three types of graphitic membranes was plotted against the inverse of the film thickness, shown in Fig. 3b. Permeance in GPU is the volumetric flow rate per unit area per unit pressure difference. Figure 3b shows that the volumetric flow rate through the membranes is inversely proportional to the membrane thickness. Vertical as well as horizontal slit channels are present in the graphitic film membranes that are interconnected for the flow, as illustrated in the figure 3-9. Because of the crystalline nature of the membrane, the thickness can be taken as a measure of the length of the interconnected slit channels. Thus, the volumetric flow rate is inversely proportional to the slit channel length according to the three straight lines obtained for HGF, TGF1, and TGF2 in Fig. 4-11(a), which is a major characteristic of Hagen-Poisseuille law[4] that governs the bulk laminar flow through a channel.

Another major characteristic of the law is that the volumetric flow rate is proportional to the applied pressure difference, the other factors being viscosity and channel dimensions. Figure 4-11(b) indicates that the CO_2

permeance is practically constant when the applied pressure is varied from 1 bar to 20 bar, which means that the volumetric flow rate is proportional to the pressure difference. Compliance with the law with respect to the applied pressure is another indication that the CO_2 flow in the graphitic film has the characteristics pertinent to Hagen-Poisseuille flow. Similar flow behavior was observed for the other graphitic membranes of TGF1 and HGF.

The usual mechanism of flow through the membranes with molecular selectivity is sorption-diffusion. The kinetic diameters of carbon dioxide and nitrogen are 3.3 and 3.6 angstroms. Considering that the slit channel height in the graphitic membranes is smaller than 4.0 angstroms, there cannot be two layers of gas molecules passing through the channels. Hence, it is a single-file flow involving only one molecular layer. This single-file flow, according to the findings, has the traits of Hagen-Poisseuille flow.

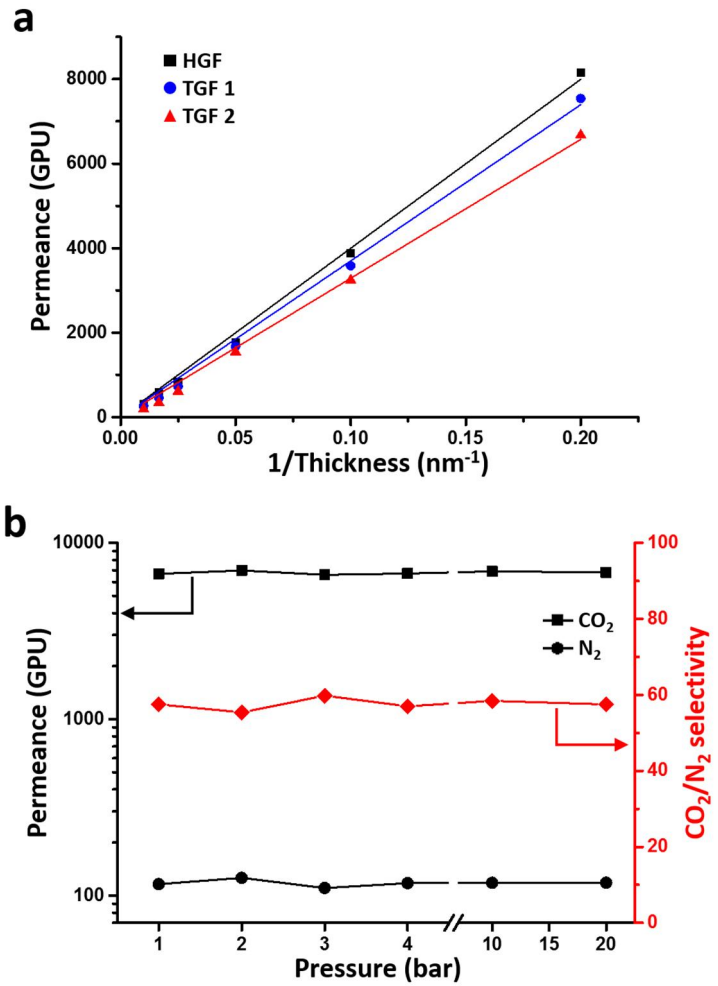

Figure 4-11. (a) Permeance as a function of the inverse of the membrane thickness for HGF, TGF1, and TGF2. (b) Permeance of CO_2 and N_2, and CO_2/N_2 selectivity plotted against applied pressure difference for TGF2 membrane 5 nm thick.

4.3.2. CO_2/CH_4 separation

The results obtained so far motivated us to look into CO_2/CH_4 pair that is relevant to natural gas and bio-gas purification. The experimental results for the CO_2/CH_4 pair are given in Fig. 4-12 in terms of selectivity and permeance attainable with TGF2 film for various film thicknesses ranging from 5 nm to 100 nm. Here again, as was the case with the CO_2/N_2 pair, the selectivity is practically unaffected by the permeance when the TGF2 film thickness is decreased for higher permeance. The selectivity attainable by the graphitic film far exceeds any reported to date, as shown in the figure.

The membranes typically used for CO_2 removal from natural gas are known to lose much of their selectivity at the high pressure (20 to 60 bar) encountered in the processing, and fresh composite membranes lose 25% of their permeance within a few days. The polymeric membrane incorporating MOF nanocrystals is also sensitive to pressure. In this light, the graphitic films were tested for its sensitivity to variations in temperature, pressure, and time. Neither the permeance nor the selectivity was affected much by

the applied pressure, as shown in figure 4-13(a). Both the selectivity and the permeance of the graphitic film remained relatively constant during a period of 48 hours (figure 4-13(b)). Insensitivity to variations in temperature is also demonstrated in figure. These robust characteristics could be attributed to the graphitic nature of the membranes.

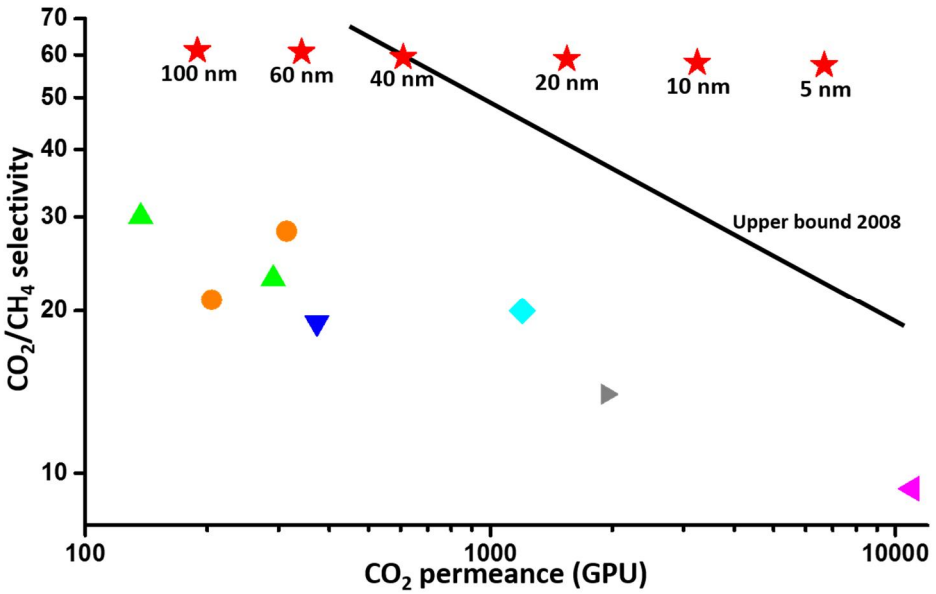

Figure 4-12. CO_2/CH_4 selectivity and the corresponding permeance for various film thicknesses of the membranes ranging from 5 nm to 100 nm (red stars), compared with literature data. The line in the figure shows the Robeson upper bound [130-136].

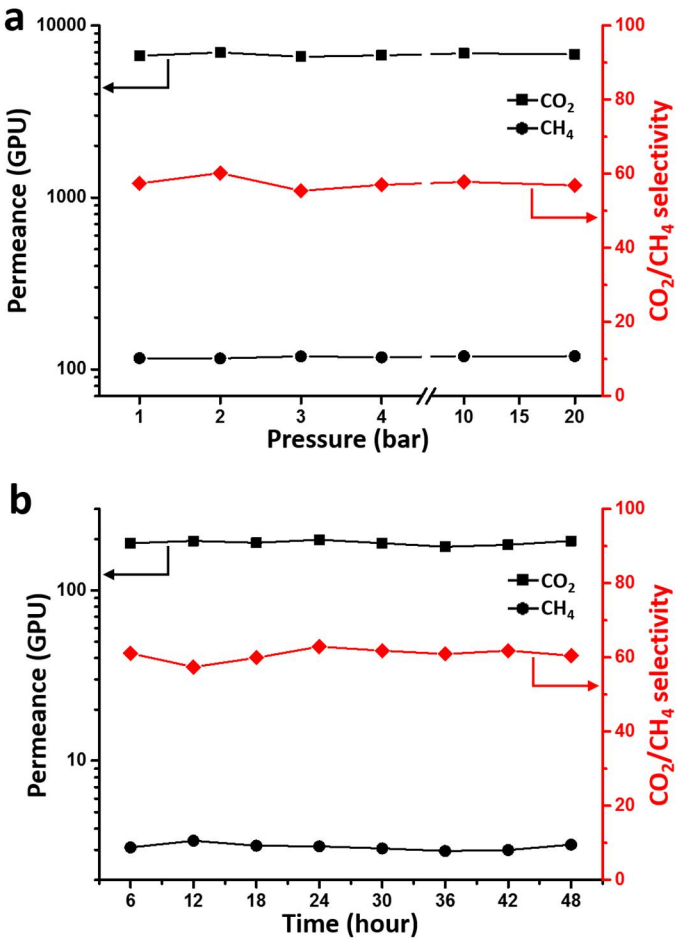

Figure 4-13. (a) CO_2 permeance and selectivity plotted against applied pressure for the film 5 nm thick. (b) Time dependence of permeance and CO_2/CH_4 selectivity for the film 100nm thick.

Chapter 5. Liquid separation property

Water is one of the important factors that deteriorate the performance of a cell driven by an electrolyte such as a lithium ion battery. Water dissolved in the electrolyte creates a solid interface between the electrolyte and the electrode, which interferes with the contact between the electrolyte and water, thereby deteriorating the performance of the battery. Therefore, it is important to prepare an electrolyte having a low water content to maintain battery performance. The technique of removing water from the electrolyte is complicated and requires large equipment, but the graphitic film produced in this study can be used to easily separate electrolyte and water.

5.1. Background of liquid separation

5.1.1. Electrolyte in Li-ion battery

Li-ion batteries use various electrolytes of carbonate series. For example, electrolytes such as ethylene carbonate (EC), dimethyl carbonate (DMC), ethylmethyl carbonate (EMC), diethyl carbonate (DEC) and propylene carbonate (PC) are used. As shown in table 4, various electrolyte are used in combination, and LiF_6 is used as a salt to drive the battery.

However, LiF_6 is vulnerable to water, so electrolytes must always have low water content. As shown in table 4, all electrolytes should always maintain a water content of less than 15 ppm. If it does not, the water dissolved in the electrolyte will degrade the salt and adversely affect battery performance.

To solve this problem, a technique for separating electrolyte and water has been researched and developed. However, complex multi-stage equipment is needed because it removes water through multi-stage filtration equipment or distillation (figure 5-1) [137-139].

Table 4. Variable electrolytes used in a Li-ion battery.

Composition	Electrolyte Salt	Appearance	Moisture
EC:EMC 1:1	$LiPF_6$ 1M	Colorless	<15 ppm
EC:DMC:EMC (2:2:1)	$LiPF_6$ 1M	Colorless	<15 ppm
EC:DMC:EMC (3:3:4)	$LiPF_6$ 1M	Colorless	<15 ppm
EC:DEC:EMC (1:1:1)	$LiPF_6$ 1M	Colorless	<15 ppm

Figure 5-1. Large equipment to remove electrolyte dissolved in water.

5.1.2. Water impurity in electrolyte

Previously, numerous of researchers revealed that the water uptake absorbed in the electrolyte or the electrodes, causing some of enormous pernicious effects on lithium ion battery such as capacity, cycle life and safety. It is commonly accepted that the moisture in $LiPF_6$-based electrolyte generating irreversible side reaction which makes energy density loss due to the water has been reacted with $LiPF_6$ and produced inorganic solid electrolyte interfaces (SEIs) on the anode surface and HF in the electrolyte. Therefore, it needs strict domination of the forming mechanism of SEIs such as chemical composition, film thickness and electrode surface morphology concerning battery performances (figure 5-2(a-b)).

The performance improvement regarding the amount of water uptake on lithium ion batteries obeying a novel additive in the electrolyte has been examined. The full cell initial capacity with optimum moisture content of the additive in the electrolyte is 100-130 ppm and brings about more than 144 mAh/g compare to those without additive. The reaction mechanisms of additive with water in the batteries are going to be revealed in this work.

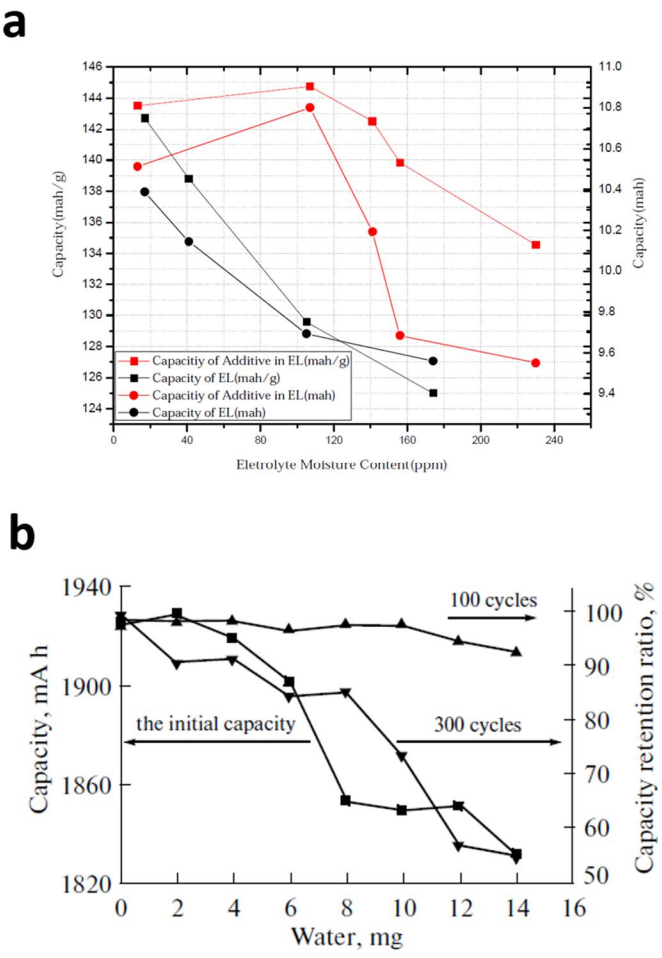

Figure 5-2. (a) The capacities relationship of the w/wo additive and moisture content in the electrolyte in lithium batteries (b) The initial capacities and cycling behaviors for batteries contained different dosage of water.

Lithium ion batteries have received considerable attention over the last two decades because of their high energy density. Li batteries are fabricated in a low-humidity environment to prevent atmospheric moisture from reacting with the lithium ions in the electrolyte. In addition, electrodes having excessively high water contents are also liable to undergo a gas liberating electrolysis reaction during operation. According to the related literature, the lithium salt in the electrolyte is dissociated according to the following two equations (figure 5-3). However, the lithium single ion (Li^+) and the Lewis acid (PF_5) easily react with water to produce HF and other unwanted products. Therefore, water is conventionally regarded as being detrimental to lithium batteries. The following equations demonstrate the reactions that occur inside the lithium ion battery, leading to its inferior performance [140-141].

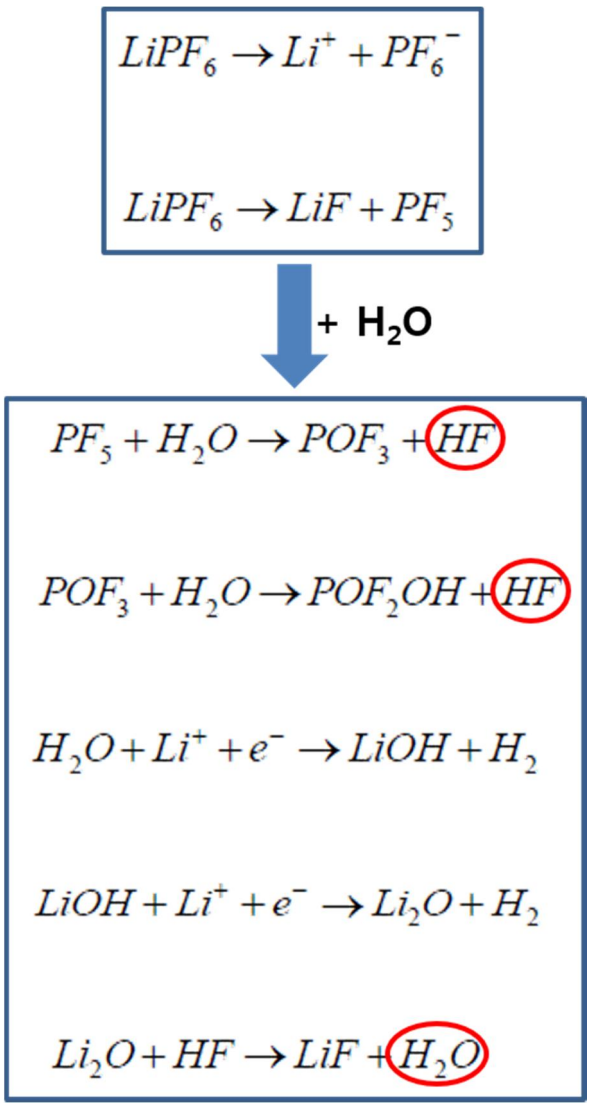

Figure 5-3. Equations between water and LiF_6.

5.2. Liquid separation performance

5.2.1. Experimental set-up

Figure 5-4(a) shows the fabrication process of a filter for separating water from water and oil or electrolyte using graphitic film made with CVHT process. The basic support of the filter was made to pass through the graphitic film through the glass filter without any degradation. On top of this, a nylon filter to support the graphitic film was placed and the graphitic film was closed around with epoxy to allow the solution to pass through the graphitic film only.

Various oils and electrolytes were tested and the water content of the permeated solution was measured using a Karl fischer coulometer. It is possible to measure the water content of 10 ppm or less, so that it is possible to carry out an accurate reliability test.

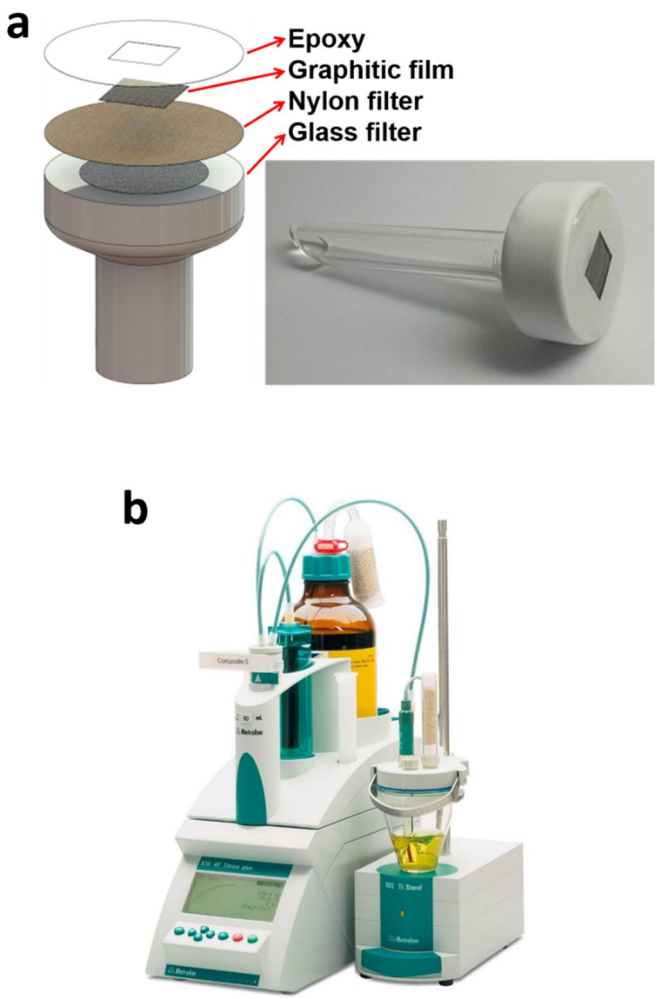

Figure 5-4. (a) Preparation of a graphitic membrane filter. (b) Image of Karl fischer coulometer

5.2.2. Intrusion pressure

The graphitic films with good alignment showed that the permeated solution was permeated quickly but the permeable solution could not permeate even when pressurized. Since the CVHT process for producing graphitic films utilizes the reduction of GO, the produced films have hydrophobic properties. Therefore, it was confirmed that the organic solvent rapidly penetrates into the film. However, even under the negative pressure pulling under the graphitic film, water was not observed at all (Fig. 5-5).

This property can be attributed to the excellent alignment of the graphitic film. The graphitic film of this structure can prevent the permeation of water even under high pressure. The intrusion pressure presented in the existing literature is shown in Figure 5-5 (b). Films permeable to water or organic solvents have low intrusion pressures due to the use of porous materials (left side of figure 5-6 (b)). On the other hand, the graphitic film developed by the present research team confirmed that water was not permeated even

when water was pushed at a high pressure of 10 bar (right side of figure 5-6 (b)).

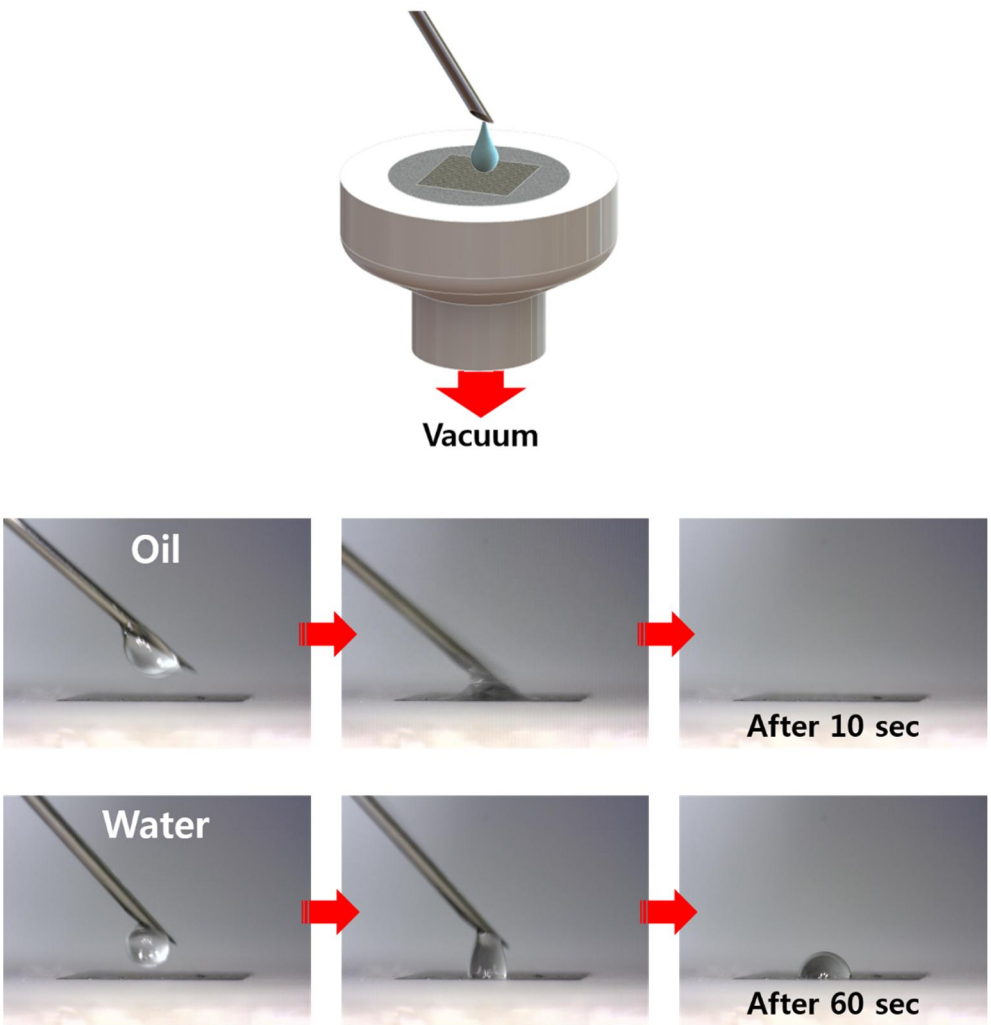

Figure 5-5. Hydrophobic and oleophilic characteristics of graphitic film.

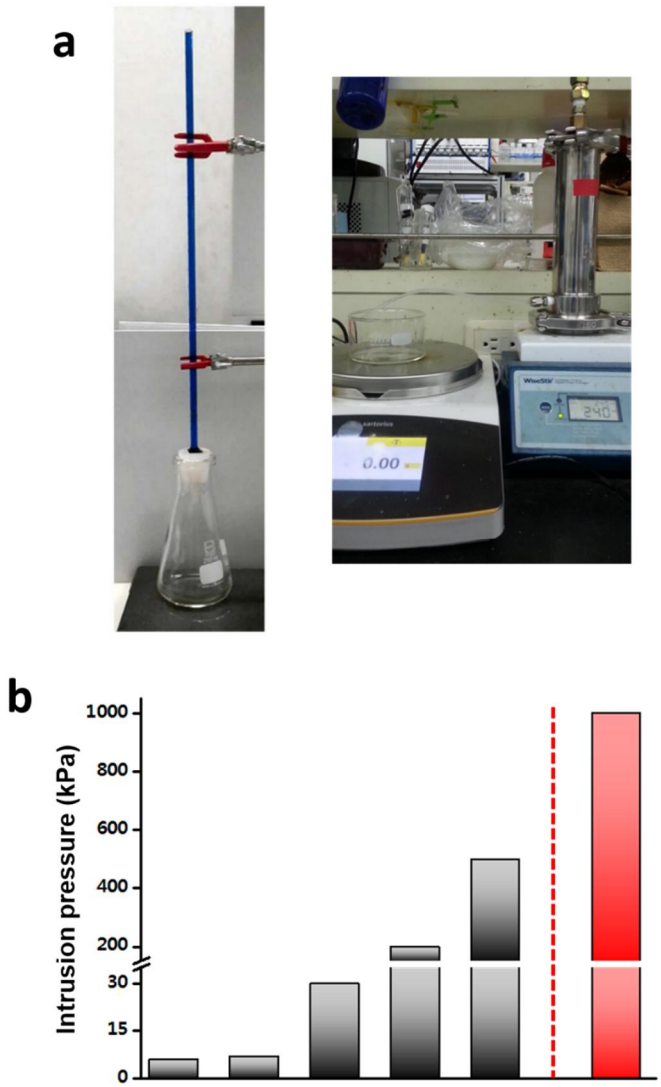

Figure 5-6. (a) Images of intrusion pressure test. (b) Comparison of intrusion pressure values of other literature [142-146].

5.2.3. Separation performance of variable oils

Separation performance for various oils, organic solvents and electrolytes was confirmed. The mixed solution was prepared by mixing the solvent and water at a ratio of 1:1, and then the solvent was permeated through vacuum filtration. The water content in the permeated solvent was measured, and the permeability was calculated by measuring the permeation amount when permeated.

It was confirmed that all the solvents had a water content of 10 ppm level. This is similar to the level of purification of solvents using existing large-scale equipment. In addition, it confirmed that it has a high permeation rate of 2000 LMH level, and confirmed the possibility of commercializing the filter.

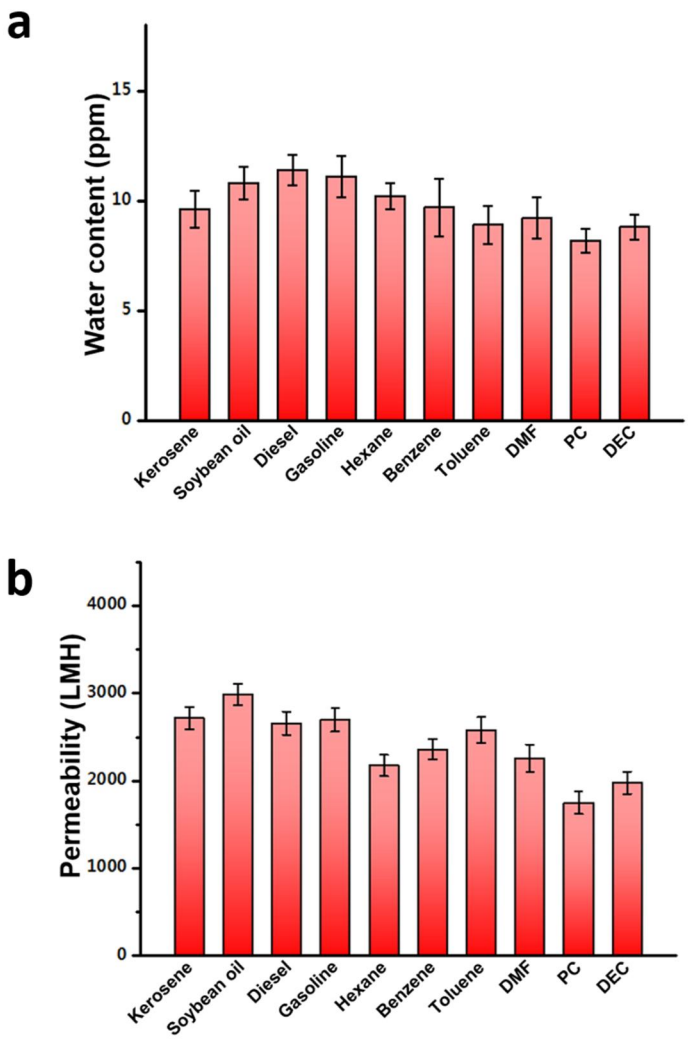

Figure 5-7. (a) Water content of variable oils. (b) Permeability of variable oils.

5.2.4. Separation performance of electrolytes

The water removal efficiency of graphitic films was measured by using PC and DEC, which are typical electrolytes used in lithium ion batteries, as a solvent. Figure 5-8 (a) shows that more than 10 ppm of water is dissolved in the newly purchased PC and DEC. When the water is removed by using a vacuum filtration method, the water content of the electrolyte drops below 10 ppm.

In addition, experiments were conducted to remove moisture through filtration of a mixture made by forcibly mixing water and electrolyte. Since it is an electrolyte having a high water solubility, it has been confirmed that when water is dissolved in an electrolyte, it has a water content of 2000 ppm or more. Filtration of the electrolyte with a high water content resulted in a water content below 10 ppm (Fig. 5-8 (b)). It was confirmed that the filter made by using graphitic film has excellent performance.

In addition, it was confirmed that the water content was lowered by continuous filtration of the solvent (Fig. 5-9 (a)). It was confirmed that the

water content was saturated when the step 6 was repeated. In order to confirm the chemical safety of the filter, the experiment was performed using water having various acidity, and the performance of the filter was confirmed to be unaffected by the pH of the water (Fig. 5-9 (b)).

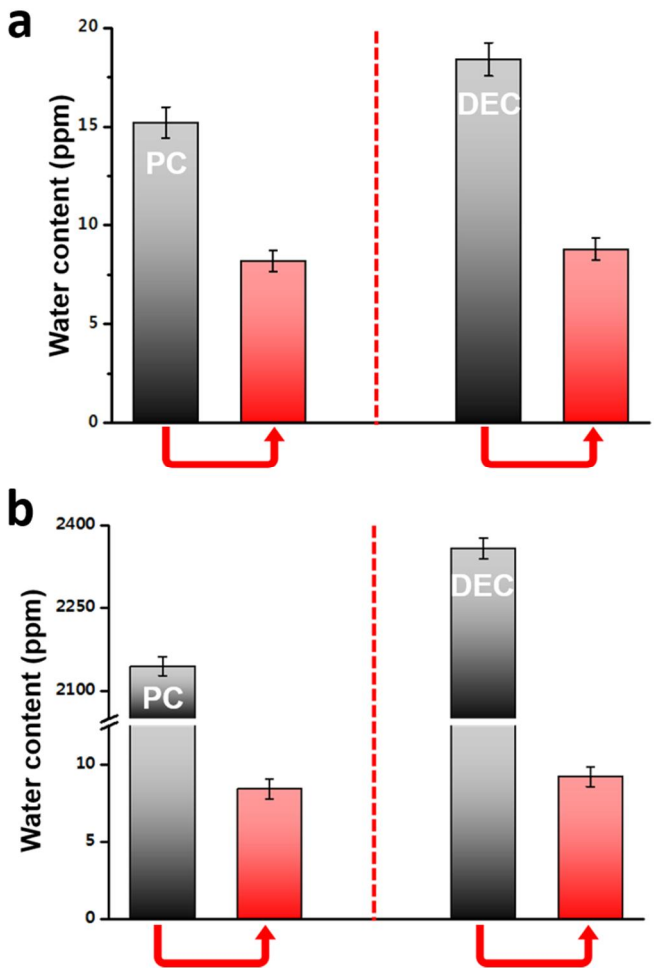

Figure 5-8. (a) Water content of electrolytes after filtration of new electrolytes. (b) Water content of electrolytes after filtration of electrolyte-water mixtures.

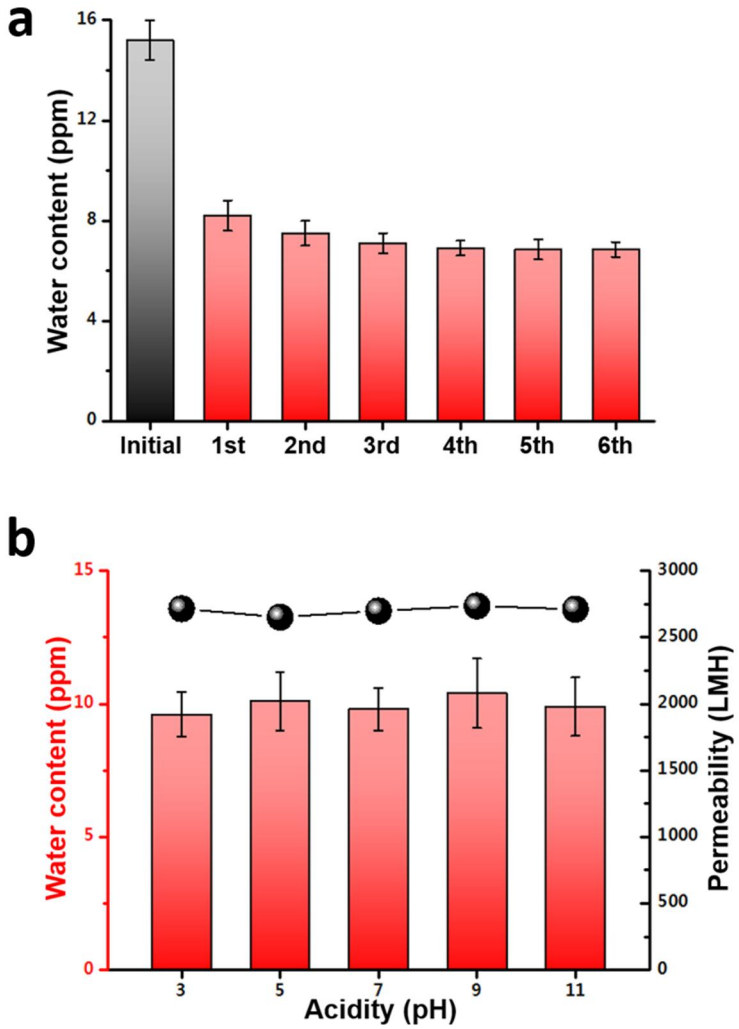

Figure 5-9. (a) Water content of electrolyte after cycling filtration. (b) Water content of electrolyte about acidity test.

Chapter 6. Conclusions

The synthesized graphitic membranes are a whole body of chemically bonded graphenic nanosheets whereas GO membranes are a simple physical mixture of GO nanosheets laminated by filtration. More importantly, permeation is through nanopores created by the edges of non-interlocked GO sheets or through structural defects within GO flakes for the GO membranes whereas the molecule movement is through the whole cross-section of slit channels for the graphite-emulating graphitic membranes.

Graphite could be an ideal molecular sieve for high permeance, provided the intra-slits are interconnected and molecules can pass through the outermost surface. The interlayer spacing provides the size for the selective molecular sieving. The one-carbon atom thick layer separates successive slit channels such that the whole cross section of the membrane is open for passage of fluid except for the space occupied by the mono-atomic layers separating the slits. Therefore, it has the maximum possible cross-sectional pore area

for high permeance while maintaining the molecular selective sieving capability.

The graphitic membranes synthesized here are fairly close to the ideal structure except that the access to the open slits is through the interconnected rGO nanosheets on the top surface. Any attempt to synthesize a membrane that is graphitic in nature would improve the permeance with little loss of selectivity, advancing the graphitic membranes as a class of molecular-sieving membranes distinct from those based on synthesized zeolite, MOF, and polymer composites.

Bibliography

[1] A. K. Geim et al., Nat. Mater. 2007, 6, 183.

[2] S. V. Morozov et al., Phys. Rev. Lett. 2008, 100, 016602.

[3] C. Lee et al., Science 2008, 321, 385.

[4] X. Li et al., Nano Lett. 2009, 9, 4359.

[5] H. P. et al., Z. Anorg. Allg. Chem. 1962, 316, 119.

[6] J. Wintterlin et al., Surf. Sci. 2009, 603, 1841.

[7] A. J. Vanbommel et al, Surf. Sci. 1975, 48, 463.

[8] X. Liu et al., Nano Lett. 2012, 12, 1013.

[9] V. Singh et al, Prog. Mater. Sci. 2011, 56, 1178.

[10] N. O. Weiss et al, Adv. Mater. 2012, 24, 5782.

[11] A. Ambrosi et al, Chem. Rev. 2014, 114, 7150.

[12] D. R. Dreyer et al., Angew. Chem. Int. Ed. 2010, 49, 9336; Angew. Chem. 2010, 122, 9524.

[13] Y. Hernandez et al., Nat. Nanotechnol. 2008, 3, 563.

[14] X. S. Li et al, Science 2009, 324, 1312.

[15] S. Stankovich et al., Nature 2006, 442, 282.

[16] D. A. Dikin et al., R. S. Ruoff, Nature 2007, 448, 457.

[17] S. Park et al, Nat. Nanotechnol. 2009, 4, 217.

[18] D. W. Boukhvalov et al., J. Phys. Condens. Matter. 2009, 21.

[19] M. J. Allen et al, Chem. Rev. 2009, 110, 132.

[20] C. N. R. Rao et al, Angew. Chem. Int. Ed. 2009, 48, 7752.

[21] J. Kang, et al, Nanoscale 2012, 4, 5527.

[22] Y. Gong et al., Adv. Funct. Mater. 2012, 22, 3153.

[23] A. Ambrosi et al., Nanoscale 2014, 6, 472.

[24] K. Parvez et al., J. Am. Chem. Soc. 2014, 136, 6083.

[25] C. T. J. Low et al., Carbon 2013, 54, 1.

[26] J. Wang et al., J. Am. Chem. Soc. 2011, 133, 8888.

[27] A. J. Cooper et al., Carbon 2014, 66, 340.

[28] A. C. Ferrari et al., Phys. Rev. Lett. 2006, 97, 187401.

[29] D. R. Dreyer et al., Chem. Soc. Rev. 2010, 39, 228.

[30] K. P. Loh et al., J. Mater. Chem. 2010, 20, 2277.

[31] A. Fasolino et al., Nat. Mater. 2007, 6, 858.

[32] J. C. Meyer et al., Nature 2007, 446, 60.

[33] A. Deshpande et al., Phys. Rev. B 2009, 79, 205411.

[34] M. L. Teague et al., Nano Lett. 2009, 9, 2542.

[35] K. Xu et al., Nano Lett. 2009, 9, 4446.

[36] A. Hashimoto et al., Nature 2004, 430, 870.

[37] J. C. Meyer et al, Nature 2008, 454, 319.

[38] W. Scholz et al., Z. Anorg. Allg. Chem. 1969, 369, 327.

[39] A. Dimiev et al., J. Am. Chem. Soc. 2012, 134, 2815.

[40] A. Ambrosi, et al., Chem.–Eur. J. 2011, 17, 10763.

[41] R. Muszynski et al., J. Phys. Chem. C 2008, 112, 5263.

[42] Y. Si et al., Nano Lett. 2008, 8, 1679.

[43] C. K. Chua et al., J. Mater. Chem. A 2013, 1, 1892.

[44] A. Ambrosi et al., Chem. Mater. 2012, 24, 2292.

[45] P. Cui et al., Chem. Commun. 2011, 47, 12370.

[46] Y. B. Zhang et al., Nature 2005, 438, 201.

[47] F. Schedin et al., Nat. Mater. 2007, 6, 652.

[48] X. Du et al., Nat. Nanotechnol. 2008, 3, 491.

[49] V. P. Gusynin et al., Phys. Rev. Lett. 2005, 95, 146801.

[50] N. M. R. Peres et al., Physical Review B 2006, 73, 125411.

[51] D. L. Miller et al., Science 2009, 324, 924.

[52] V. M. Apalkov et al., Phys. Rev. Lett. 2006, 97, 126801.

[53] X. Du et al., Nature 2009, 462, 192.

[54] S. V. Morozov et al., Phys. Rev. Lett. 2006, 97, 016801.

[55] N. Stander et al., Phys. Rev. Lett. 2009, 102, 026807.

[56] C. D. Reddy et al., Nanotechnology 2006, 17, 864.

[57] A. Ambrosi et al., Chem. Eur. J. 2011, 17, 10763.

[58] A. Ambrosi et al., Chem. Sus. Chem. 2014, 7, 1102.

[59] A. Ambrosi et al., Chem. Mater. 2012, 24, 2292.

[60] Y. Zhu et al., Adv. Mater. 2010, 22, 3906.

[61] A. Bonanni et al., Chem. Eur. J. 2014, 20, 217.

[62] X. Huang et al., Chem. Soc. Rev. 2012, 41, 666.

[63] A. J. Patil et al., Adv. Mater. 2009, 21, 3159.

[64] P. H. Chen et al., Anal. Chem. 1995, 67, 3115.

[65] T. J. Davies et al., Angew. Chem. Int. Ed. 2005, 44, 5121.

[66] X. B. Ji et al., Chem. Phys. Chem. 2006, 7, 1337.

[67] S. J. Konopka et al., Anal. Chem. 1970, 42, 1741.

[68] G. Van Lier et al., Chem. Phys. Lett. 2000, 326, 181.

[69] P. Guo et al., Electrochem. Commun. 2009, 11, 1320.

[70] H. Chen et al., Adv. Mater. 2008, 20, 3557.

[71] N. M. R. Peres, J. Phy. Condens. Matter 2009, 21.

[72] F. Wang et al., Science 2008, 320, 206.

[73] F. Rana et al., Phys. Rev. B 2009, 79, 115447.

[74] V. C. Tung et al., Nat. Nanotechnol. 2009, 4, 25.

[75] X. Zhou et al., J. Phys. Chem. C 2011, 115, 11957.

[76] S. Mao, et al., Nanoscale 2011, 3, 2849.

[77] T. Sakura et al., Colloid Polym. Sci. 2007, 285, 1407.

[78] S. Liu et al., Carbon 2011, 49, 3158.

[79] J. F. Che et al., J. Mater. Chem. 2010, 20, 1722–1727.

[80] Z. Lei et al., Energy Environ. Sci., 2012, 5, 6391.

[81] X. P. Shen et al., J. Colloid Interface Sci. 2011, 354, 493.

[82] D. R. Dreyer et al., J. Mater. Chem., 2011, 21, 3443.

[83] G. Wang et al., J. Phys. Chem. C 2008, 112, 8192.

[84] J. Gao et al., Chem. Mater., 2010, 22, 2213.

[85] C. Zhu et al., ACS Nano 2010, 4, 2429.

[86] Y.-K. Kim et al., Chem. Commun. 2011, 47, 3195.

[87] W. Chen et al., J. Phys. Chem. C 2010, 114, 19885.

[88] Y. Liu et al., J. Nanosci. Nanotechnol., 2011, 11, 10082.

[89] S. Some et al., Sci. Rep. 2013, 3, 1929.

[90] Z. Fan et al., Carbon 2010, 48, 1686.

[91] P. Blake et al., Appl. Phys. Lett. 2007, 91, 063124.

[92] S. Roddaro et al., Nano Lett. 2007, 7, 2707.

[93] I. Jung et al., Nano Lett. 2007, 7, 3569.

[94] D. S. L. Abergel et al., Appl. Phys. Lett. 2007, 91, 063125.

[95] L. B. Gao et al., ACS Nano 2008, 2, 1625.

[96] V. Yu et al., Appl. Phys. Lett. 2009, 95, 151904.

[97] M. Bruna et al., Appl. Phys. Lett. 2009, 94, 031901.

[98] S. Piscanec et al., Eur. Phys. J. Special Topics 2007, 148, 159.

[99] L. M. Malard et al., Phys. Rep. 2009, 473, 51.

[100] J. Rohrl et al., Appl. Phys. Lett. 2008, 92, 201918.

[101] Z. H. Ni et al., Phys. Rev. B 2008, 77, 115416.

[102] J. Yan et al., Phys. Rev. Lett. 2007, 98, 166802.

[103] S. Pisana et al., Nat. Mater. 2007, 6, 198.

[104] J. A. Robinson et al., Nano Lett. 2009, 9, 2873.

[105] C. Casiraghi et al., Nano Lett. 2009, 9, 1433.

[106] X. Mei et al., Carbon 2011, 49, 5389.

[107] P. B. Liu et al., Mater. Lett. 2013, 91, 125.

[108] R. S. Dey et al., Chem. Commun. 2012, 48, 1787.

[109] V. H. Pham et al., J. Mater. Chem. 2012, 22, 10530.

[110] B. K. Barman et al., RSC Adv. 2013, 3, 12621.

[111] Y. Liu et al., J. Mater. Chem. 2011, 21, 15449.

[112] S. Yang et al., RSC Adv. 2012, 2, 8827.

[113] H. Feng et al., Nat. Commun. 2013, 4, 1539.

[114] D. Chen et al., Nanotechnology 2011, 22, 325601.

[115] J. K. Ma et al., J. Mater. Chem. A 2013, 1, 2192.

[116] T. A. Pham et al., Colloids Surf. A 2011, 384, 543.

[117] Y. Wang et al., ACS Appl. Mater. Interfaces 2011, 3, 1127.

[118] S. Thakur et al., Carbon 2012, 50, 5331.

[119] B. Haghighi et al., RSC Adv. 2013, 3, 13365.

[120] E. C. Salas et al., ACS Nano 2010, 4, 4852.

[121] G. Wang, et al., Nano Res. 2011, 4, 563.

[122] S. Gurunathan, et al., Colloids Surf. B, 2013, 102, 772.

[123] C. H. Yu et al., Nano Lett. 2005, 5, 1842.

[124] D. L. Nika et al., Phys. Rev. B 2009, 79, 155413.

[125] Z. Guo et al., Appl. Phys. Lett. 2009, 95, 163103.

[126] I. K. Hsu et al., Nano Lett. 2009, 9, 590.

[127] J. H. Seol et al., Science 2010, 328, 213.

[128] H. B. Heersche et al., Nature 2007, 446, 56.

[129] Y. M. Lin et al., Nano Lett. 2009, 9, 422.

[130] L. A. Ponomarenko et al., Science 2008, 320, 356.

[131] S. Y. Zhou et al., Nat. Mater. 2007, 6, 770.

[132] J. B. Oostinga et al., Nat. Mater. 2008, 7, 151.

[133] Y. B. Zhang et al., Nature 2009, 459, 820.

[134] Y. W. Son et al., Phys. Rev. Lett. 2006, 97, 216803.

[135] M. Y. Han et al. , Phys. Rev. Lett. 2007, 98, 206805.

[136] X. L. Li et al., Science 2008, 319, 1229.

[137] J. R. Williams et al., Science 2007, 317, 638.

[138] D. A. Abanin et al., Science 2007, 317, 641.

[139] X. R. Wang et al., Science 2009, 324, 768.

[140] Y. P. Dan et al., Nano Lett. 2009, 9, 1472.

[141] R. Shah et al., Mater. Res. Innovations 2015, 19, 97.

[142] Z. Wang et al., Adv. Mater. 2012, 24, 3134.

[143] C. K. Chua et al., Chem. Soc. Rev. 2014, 43, 291.

[144] Z. Yang et al., Water Res. 2013, 47, 3037.

[145] J. Liu et al., AIP Adv. 2015, 5, 117151.

[146] H. Bi et al., Sci. Rep. 2013, 3, 2714.

초 록

지구 온난화, 대기 오염, 물 오염에 의한 식수원 고갈 등의 전세계가 직면하고 있는 환경 위기를 해결하기 위한 방안 중에서 가장 대표적인 기술이 멤브레인이다.

멤브레인 기술이란 혼합되어 있는 가스 또는 용액을 원하는 물질만 선택적으로 분리하는 것을 의미한다. 분리의 원리는 물리적, 화학적, 기계적 등의 다양한 원리를 이용한다. 주로, 혼합된 물질의 크기 차이를 이용한 선택적 분리 기술이 이용된다.

수많은 공장에서 생산되는 폐수의 분리 또는 사고로 바다에 유출되는 기름의 회수를 위해서는 물과 기름을 선택적으로 투과시킬 수 있는 멤브레인의 개발이 필요하다. 이와 같이 물과 기름을 분리해야 되는 상황은 빈번하게 발생하고, 깨끗한 환경 보전에 반드시 필요한 기술이다.

환경 오염이 심각해지면서 사람이 마실 수 있는 있는 식용수의 양이 줄어들고 있고, 지구온난화 등의 환경 재앙에 의해 새로운 식용수의 생산 기술 개발이 절박한 상황이다. 지구의 97 %를 차지하고 있는 해수를 담수로 바꾸는 기술은 현재뿐만 아니라 미래에 필수적인 기술이라 할 수 있다. 이에, 염을 거를 수 있는 고성능의 멤브레인의 개발이 절박하다.

또한, power plant 등에서 발생하는 유해 가스는 대부분 CO_2로 이루어져있고, CO_2는 지구온난화의 주범으로 대기 중에서 반드시 분리

및 포집을 해야한다. 그러므로 다양한 기체 분자 중에서 CO_2와 같이 원하는 기체만 분리할 수 있는 멤브레인의 제작 기술의 개발이 절실한 상황이다.

이와 같이 다양한 응용성을 가지는 고성능의 멤브레인 기술의 개발이 반드시 필요하고, 본인은 멤브레인으 성능을 향상시키기 위하여 CVHT process를 개발하였다. 이 공정을 이용하면 우수한 정렬성을 가지면서 graphene의 화학적 결합으로 인한 film을 제작할 수 있다. 이와 같이, 매우 우수한 구조의 graphitic film을 이용하여 가스와 용액을 분리할 수 있는 고성능의 멤브레인을 제작하였다.

주요어: 그래핀, 그래핀 옥사이드, 수열, 과열 증기 수열, 가스 분리, 용매 분리

학 번: 2010-30965